Enter authors here: Yuki Kita[1,2], Takuji Waseda[3]

[1] Institute of Industrial Science, The University of Tokyo, Tokyo, Japan.

[2] Gaia Vision Inc., Tokyo, Japan.

[3] Department of Ocean Technology Policy and Environment, Graduate School of Frontier Science, The University of Tokyo, Chiba, Japan.

Corresponding author: Yuki Kita (ykita@rainbow.iis.u-tokyo.ac.jp)

Key Points:

- The ocean waves enhanced the sea surface sensible and latent heat supply and intensified the development of the explosive cyclone.
- A fully atmosphere-ocean-wave coupled model with the effect of ocean surface waves improved the reproducibility of the explosive cyclone.

Abstract

Atmosphere-ocean interactions are thermodynamically important in the development of explosive cyclones. An explosive cyclone which emerged in the Northwestern Atlantic in January 2018 received massive heat from the Gulf Stream and developed rapidly due to enhanced atmospheric instability. Ocean surface waves affect momentum and heat air-sea exchanges, but their roles in explosive cyclone development have not been examined. This study shows that waves enhance the development of the explosive cyclone using a coupled atmosphere-ocean-wave model. The developing waves increased sensible and latent heat supply by increasing the transfer coefficient and friction under the cyclone. The increased heat supply from the sea surface strengthened the convective instability in the lower atmosphere. The air was lifted to the middle troposphere near the bent-back front by a strong updraft and enhanced precipitation near the cyclone's center. The resulting latent heat release produced positive potential vorticity in the lower troposphere and intensified the explosive cyclone development. Waves also enhanced vertical ocean mixing, and sea surface temperature (SST) warmed north of the Gulf Stream. Overall, the most dominant effect of waves for the explosive cyclone development was to increase the supply coefficients of sensible and latent heat. Introducing ocean surface waves into the numerical simulations improved the reproducibility of explosive cyclones, indicating the importance of waves in explosive cyclone development.

Plain Language Summary

Explosive cyclones are a type of rapidly developing extratropical cyclone influenced by the ocean; the explosive cyclone that developed in the northwestern Atlantic in January 2018 received massive heat from the Gulf Stream and developed rapidly due to atmospheric instability. Ocean surface waves are an important factor in altering the supply of heat from the sea surface, but their role in the explosive cyclone development is not well understood. In this study, we use a coupled atmosphere-ocean-wave model to show that waves can enhance

the development of explosive cyclones. Waves reduced sea level pressure more by increasing sea level friction and supplying more heat from the sea surface. The supplied heat made the lower atmosphere unstable and produced more precipitation. The waves also enhanced ocean vertical mixing, and SSTs were found to increase north of the Gulf Stream. Overall, the most dominant effect of waves was to increase the supply coefficients of sensible and latent heat. By introducing waves into the numerical simulations, the reproducibility of explosive cyclones was improved, therefore showing that waves are important for the development of explosive cyclones.

1 Introduction

An explosive cyclone is defined as a more intense extratropical cyclone whose central sea level pressure (SLP) drops by more than 24 hPa in a 24 hour period (Sanders & Gyakum, 1980). Explosive cyclones' surface wind speed and central SLP often reach values equivalent to a tropical cyclone and generate extreme ocean surface waves. They are one of the major causes of severe marine disasters such as coastal floods, ship accidents, and structural damage to offshore platforms. For example, early in January 2018, an explosive cyclone ran along the eastern coast of the U.S. and caused serious blizzards over the eastern U.S. In Massachusetts, high ocean waves have flooded large coastal areas. The total damage caused by this storm amounted to about $1.1 billion. The cyclone was ranked the most powerful winter storm in the history of the U.S.

Three possible mechanisms can rapidly intensify extratropical cyclones: upper-level forcing associated with potential vorticity anomalies, instability by energy fluxes from the ocean, and massive latent heat releases (Catto, 2016). Explosive cyclones usually emerge in the vicinity of the Gulf Stream and the Kuroshio/Kuroshio Extension. The western boundary currents supply a large amount of sensible and latent heat into the atmosphere. Many studies have pointed out that a large amount of heat supply can rapidly intensify the extratropical cyclones through increasing atmospheric instability and latent heating (e.g., Kuo et al. 1991; Reed et al. 1993; Takayabu et al. 1996; Gyakum & Danielson 2000; dal Piva et al. 2011). The sensible and latent heat supply from the sea surface rapidly develops the explosive cyclone by maintaining the vertical atmospheric circulation of the updraft region (Nuss & Kamikawa, 1990). Hirata et al. (2015, 2019) reported the detailed processes of the rapid development of explosive cyclones. First, the sensible and latent heat on the surface layer is advected to the middle troposphere (~600 hPa level) by an intense updraft along the bent-back front near the cyclone center. Then, the equivalent potential temperature increases and strengthens the diabatic heating due to vapor condensation. The resulting latent heat release produces positive potential vorticity in the lower troposphere and enhances the explosive cyclone development.

Ocean surface waves greatly influence the sensible and latent heat supply from the sea surface through sea surface roughness (e.g., Donelan et al. 1993; Oost et al. 2002; Powell et al. 2003; Donelan et al. 2004; Babanin and Makin 2008; Andreas et al. 2012). Drennan et al. (2003) confirmed that the sea surface rough-

ness is inversely proportional to the wave age, which is the ratio of wave phase speed and wind friction velocity ($c_p/u_*, c_p$: phase speed, u_* : friction velocity). The young and steep waves at a short fetch roughen the sea surface and transfer a large amount of sensible and latent heat into the atmosphere. Swells ($c_p/(u_* \cos\phi) > 1$, ϕ : relative angle of the wave to the surface wind) affect sea surface roughness as well (e.g., Sullivan et al., 2014; Mahrt et al., 2018). Patton et al. (2019) performed a large-eddy atmospheric simulation above moving ocean surface waves and proposed a correction formula of the friction velocity with wave age and wind-wave directional difference. The changes in the sea surface roughness may affect the mesoscale atmospheric circulation (e.g., Perrie et al., 2005; Zhang et al., 2006). Pianezze et al. (2018) implemented an atmosphere-ocean-wave coupled model to evaluate the impacts of the ocean surface waves on a tropical cyclone. They reported that the waves roughened the sea surface and enhanced the sensible and latent heat transfer into the atmosphere from the sea surface. Renault et al. (2012) reported that the heat and momentum flux parameterization depending on the sea surface wave showed the most skillful simulation for extratropical cyclones. Those studies imply that the ocean surface waves have essential roles in the explosive cyclone. However, because explosive cyclones are different from tropical cyclones in the high translation speed and the atmospheric fronts, it is still unknown how the ocean surface waves modify the development of an explosive cyclone.

The sea surface temperature (SST) is an important factor controlling sensible and latent heat supply from the sea surface. It is well known that the ocean surface waves intensify vertical mixing in the ocean boundary layer through interactions of pre-existing turbulence. The alternation in the ocean vertical mixing primarily changes the SST. Many previous studies have clarified that the wave-derived changes in SST affect the mesoscale atmosphere phenomena (e.g., Reichl et al., 2016; Wang & Sheng, 2016; Staneva et al., 2017; Pianezze et al., 2018; Wu et al., 2019). Stoney et al. (2017) introduced the non-breaking wave-induced mixing effect into a numerical ocean model. They found that the wave-induced mixing modified shear-induced entrainment and suppressed upwelling under a tropical cyclone, resulting in SST changes near the tropical cyclone trajectory and changing the cyclone intensity. Aijaz et al. (2017) introduced the wave-induced mixing effect into an atmosphere-ocean-wave coupled model and investigated the impacts on the underlying ocean of a tropical cyclone track. They detected significant cooling of the SST and deepening of the mixed layer depth under the tropical cyclone center, which weakened the intensity of the tropical cyclone. Many studies indicate that the wave-induced transformations in internal structures of the ocean boundary layer can weaken the intensity of tropical cyclones, which usually appear in a hot season (e.g., Wada et al., 2010; He & Chen, 2011; Toffoli et al., 2012; Zhang et al., 2018). Meanwhile, an explosive cyclone generally appears in a cold season, when the depth of the ocean mixed layer is much deeper than in a warm season. How the wave-induced transformations in ocean mixing can affect the mesoscale atmospheric phenomena like an explosive cyclone in a cold season in mid-latitude zones

remains to be elucidated.

This study aims to clarify the effects of ocean waves on the development of explosive cyclones. An atmosphere-ocean-wave coupled model is tailored to elucidate how the atmosphere-ocean-wave interactions affect the atmospheric and oceanic turbulent boundary layers and, consequently, the development of the explosive cyclone and quantitatively evaluate the ocean wave impacts on the explosive cyclone development. This study aims to analyze one representative explosive cyclone that emerged in the Northwestern Atlantic in January 2018 and brought severe disasters in the Eastern U.S.

The paper is structured as follows. Section 2 provides basic information of the explosive cyclone and the ocean's surrounding environment. Section 3 describes and explains the implementation of an atmosphere-ocean-wave coupled model to analyze the ocean wave impacts on the development of an explosive cyclone. Section 4 overviews the simulation results with the atmosphere-ocean-wave coupled model and verifies the accuracy with in-situ observations. Section 5 demonstrates the effects of the ocean waves on the evolution of the explosive cyclone with the atmosphere-ocean-wave coupled model's sensitivity experiments. Finally, Section 6 summarizes the results and interpretations obtained from the sequential analyses.

2 Overview of the Explosive Cyclone in January 2018

An explosive cyclone was generated on 03 January at the east of Florida in the Northwestern Atlantic, propagated northeastward, and rapidly developed between 18:00 UTC 03 January and 18:00 UTC 04 January when the central SLP dropped by 53 hPa from 1004 hPa to 950 hPa (NOAA 2019). The maximum deepening rate of the cyclone was 3.3 hPa/hour in the ERA-Interim reanalysis (Dee et al., 2011). Historically, there have been only two explosive cyclones with the deepening rate exceeding 3.3 hPa/hour in the Northern Hemisphere between 1979 and 2014. The track of the cyclone center and the temporal evolution of the central pressure are shown in Fig 1, according to the analysis data of Climate Forecast System Version 2 (CFSv2; Saha et al. 2014). The rapid development of the explosive cyclone occurred during 0:00 and 18:00 UTC on 04 January. The cyclone induced an intense blizzard over the East of the U.S., Canada and even in Florida, and generated storm surge along the Massachusetts Bay. The cyclone also generated extremely high waves. At the observational buoy above East Scotia Slope, 17.1 m significant wave height was observed on 05 January.

The structure of the explosive cyclone well resembled the Shapiro-Keyser model (Shapiro & Keyser, 1990). At the rapid development stage, a strong updraft occurred around the western part of the bent-back front located to the northwest of the cyclone center. Latent heating by vapor condensation intensified in the vicinity of the bent-back front and deepened the explosive cyclone development. The primary factor of the rapid development of the January 2018 explosive cyclone was the supply of sensible and latent heat from the Gulf Stream (Hirata et al., 2019). Since the sea surface states and the heat content in the ocean

boundary layer are essential factors of the rapid development of the explosive cyclone, we will investigate the SST and the ocean thermal structure.

Fig 2 displays the SST horizontal distribution and vertical cross-section of water temperature just before the explosive cyclone genesis. The explosive cyclone was generated in the warm area south of the Gulf Stream, and it propagated northward across the Gulf Stream (Fig 2a). With vertical mixing under the cyclone, SST changes depend on the ocean thermal structure. The Gulf Stream axis lies around 41 $^\circ$ N in the vertical cross-section of water temperature. In the south of the Gulf Stream, warm water stays above the cold water; we define this temperature profile as a type-T profile. On the other hand, in the north of the Gulf Stream, the cold water exists above the warm water, i.e., the thermal inversion is found; we define this type of profile as a type-I profile. Due to the presence of the Labrador Current, the type-I profile spreads north of the Gulf Stream. The boundary between the warm and cold currents is north of 41 $^\circ$ N (Fig 2b). The explosive cyclone passed over regions where the thermal profiles switched from type-T to type-I. Since the SST underlying the explosive cyclone has considerable influence on the cyclone development, we investigate the impact of the variation of the thermal profiles on the cyclone development in Section 5.3.

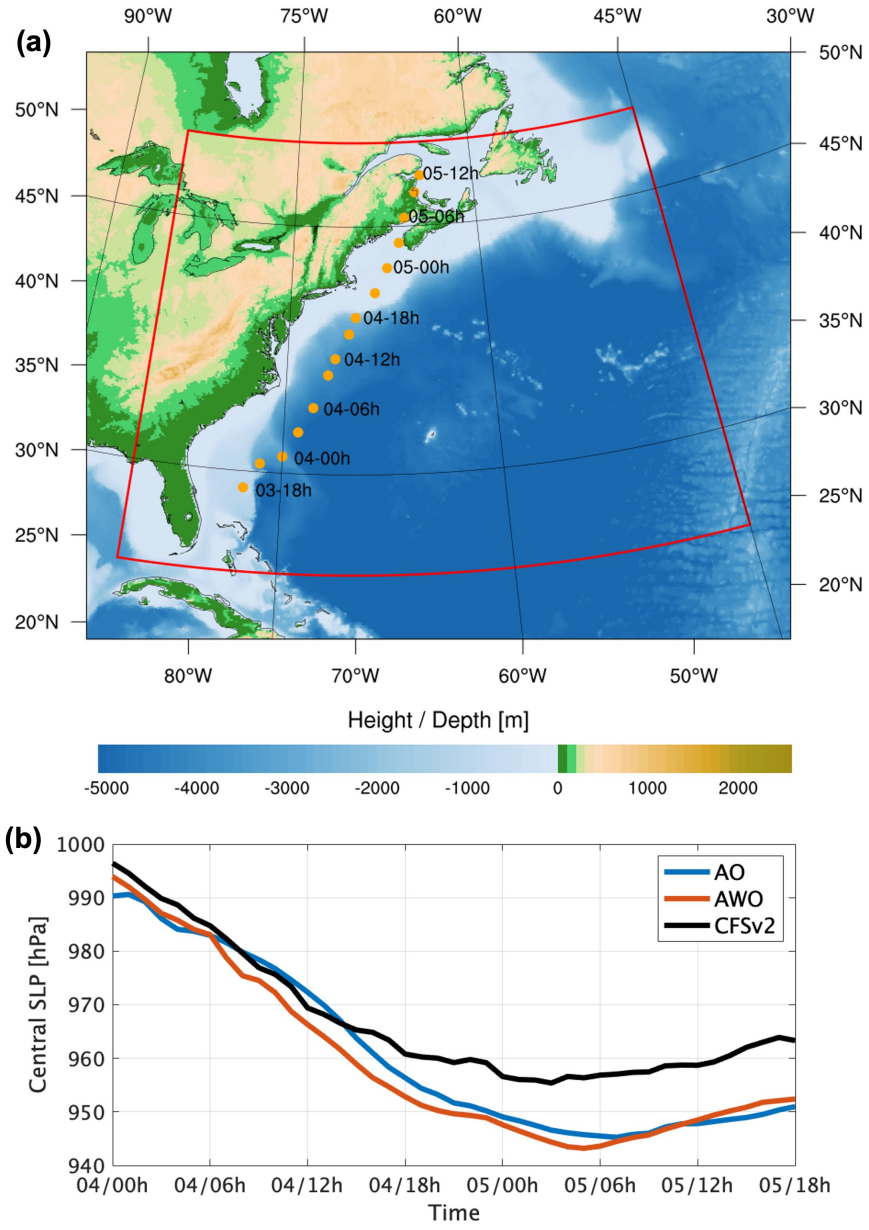

Fig 1. (top) Topography and bathymetry (m; shaded) and the trajectory (yellow dots) of the cyclone center designated by the local minimum of the sea level pressure (SLP) in CFSv2. The red line designates the calculation domain. (bottom) Time-series of the central minimal SLP [hPa] of the cyclone for the AWO (red) and the AO (blue) simulations.

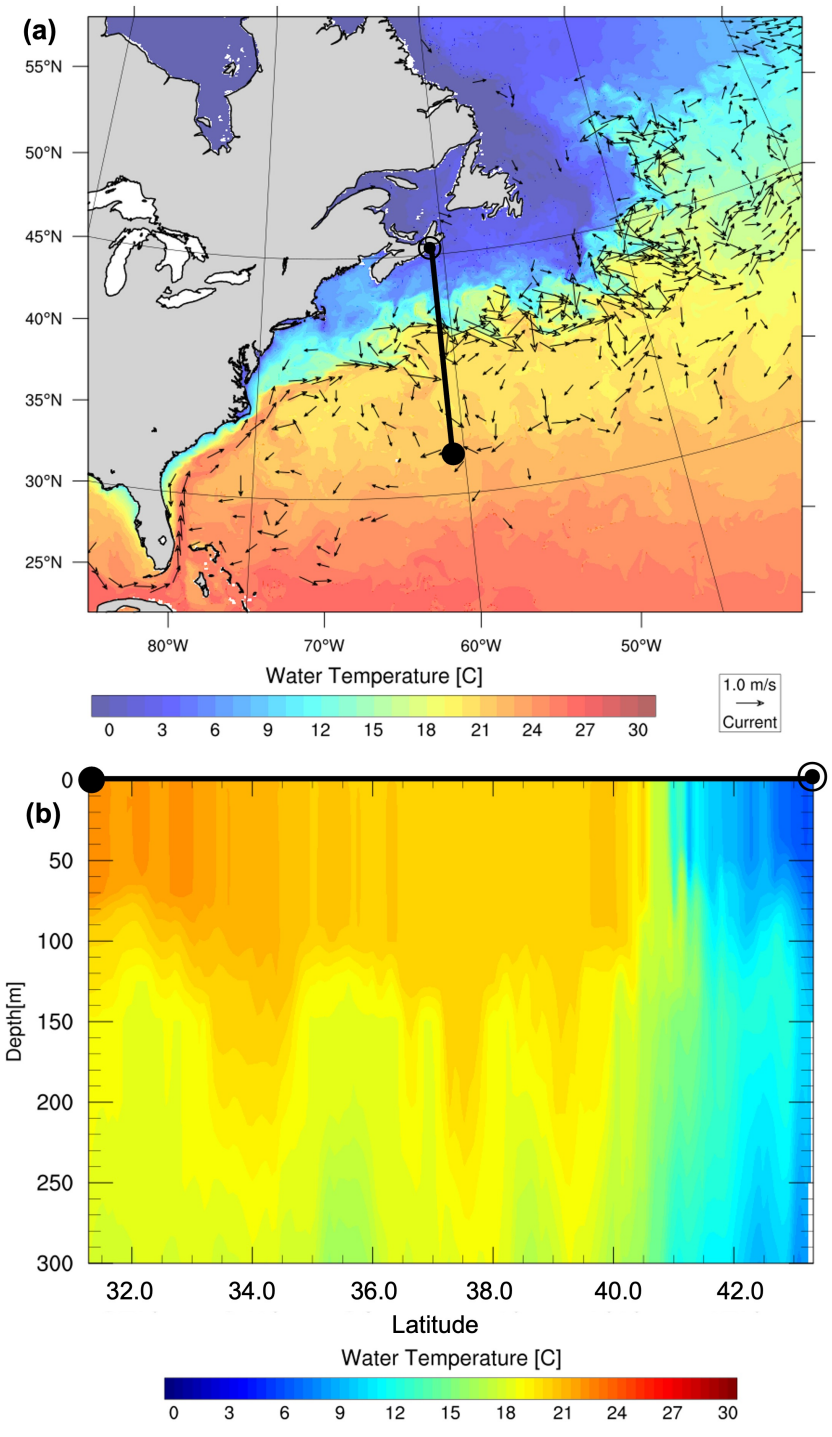
(a)
55°N
50°N
45°N
40°N
35°N
30°N
25°N
80°W
70°W
60°W
50°W
Water Temperature [C]
0 3 6 9 12 15 18 21 24 27 30
1.0 m/s
Current
(b)
0
50
100
150
200
250
300
Depth[m]
32.0
34.0
36.0
38.0
40.0
42.0
Latitude
Water Temperature [C]
0 3 6 9 12 15 18 21 24 27 30

Fig 2. (a) Horizontal distribution of SST (shaded; ℃) and surface current velocity (vector; m/s) at 0:00 UTC on 03 January in GOFSv3.1. (b) Vertical cross-section of water temperature (℃) across the black line in (a) at 0:00 UTC on 03 January.

3 Data, or a descriptive heading about data

The coupled model used in this study is composed of three components: the atmosphere model, the ocean current model, and the ocean surface wave model. This atmosphere-ocean-wave (AWO) coupled model is composed of the Weather Research and Forecasting (WRF) Model (version 3.9) as the atmosphere component model (Skamarock et al. 2008), the Coastal and Regional Ocean COmmunity model (CROCO; http://www.croco-ocean.org), and the WAVEWATCH III version 6.07 (WW3; WW3DG 2019). For variable exchange among the atmosphere-ocean-wave coupled model, the OASIS3-MCT code is used in each model program. The interval of variable coupling is every 6 minutes, which is the least common multiple of the time steps of the three models used for this coupled modeling. The calculation domain of each model is common and designated by the red line, as shown in Fig 1a. The model coupling strategy is illustrated in Section 3.4.

3-1. Model Fundamental Configuration

The WRF model is the atmospheric component of the coupled model. The governing equations are the flux-form Euler equations written with a terrain-following hydrostatic-pressure vertical coordinate. WRF provides various options of physical parameterizations for representing clouds, radiation, turbulence, microphysics, surface layer, etc. The microphysics scheme used was WRF Single-moment 6-class scheme (Hong & Lim, 2006) to predict the mixing ratio of six water categories: cloud, water vapor, cloud ice, graupel, snow, and rain. The Betts-Miller-Janjic scheme (Janjic, 1994) was used for the cumulus parameterization. The longwave radiation scheme was the Rapid Radiative Transfer Model (RRTM; Mlawer et al. 1997), and the shortwave radiation scheme was a simple downward integration scheme (Dudhia, 1989). The turbulence scheme for the planetary boundary layer was the Mellor-Yamada-Nakanishi-Niino (MYNN) 2.5 level scheme (Nakanishi and Niino 2009). For the surface layer, a revised MM5 Monin-Obukhov scheme was used (Jiménez et al., 2012). The surface sensible and latent heat flux is calculated with COARE (Coupled Ocean-Atmosphere Response Experiment; Fairall et al., 2003) version 3.0 parameterization. The horizontal grid resolution is 0.08° in both latitude and longitude with 326×501 points. It covers the region of 24~50 $^\circ$N and 85~45 $^\circ$W. The vertical grid is 60 stretched levels with an enhanced resolution close to the ground. The time-step of WRF is 30 s. The spin-up run is performed from 00:00 UTC 22 December 2017 to 00:00 UTC 01 January 2018 with the initial condition of CFSv2. The WRF experiments were forced at the lateral boundary conditions of 6-hourly CFSv2.

The CROCO model was used for the ocean component. This model is a variant

of ROMS (Regional Ocean Modeling System), originally developed by UCLA (University of California, Los Angeles). The model configuration is based on incompressible hydrostatic equations with the Boussinesq hypothesis. The model grid system consists of a horizontal Cartesian coordinate and a vertical terrain-following coordinate. The domain covers the same area as the WRF domain with the horizontal resolution of $1/18^\circ$ in both latitude and longitude with 729×597 points. The temporal discretization used was a third-order time-splitting scheme with baroclinic and barotropic time steps of 360 s and 9 s, respectively. The bathymetry was built from the ETOPO2v2 with a two arc-minute global. The vertical levels were divided into 45 layers with an enhanced resolution near the upper ocean surface. The highest layer thickness was about 2 m. The minimum depth is set as 20 m. The initial and boundary conditions are constructed from GOFS (Global Ocean Forecasting System) 3.1 analysis output (available online at https://www.hycom.org/dataserver/gofs-3pt1/analysis) developed by the NRL (Naval Research Laboratory) in the U.S. with two days interval.

For the ocean surface wave component, the WW3 model was used. Propagating free surface waves in water with limited depth and currents are generally described with amplitude and phase. WW3 solves the spectral action density balance equation with random phases for selected wavenumber-direction spectra. The third-order scheme by Tolman (2002) was used to calculate the wave propagation. The nonlinear wave-wave interactions were modeled with the Discrete Interaction Approximation (DIA, Hasselmann, et al. 1985). The wind-wave interaction is modeled and parameterized following Ardhuin et al. (2010). The bottom friction source term based on the SHOWEX experiments was used by Ardhuin et al. (2003), and the depth-induced wave breaking was modeled with the way of Battjes & Janssen (1978). The WW3 simulation domain corresponds to the domains of WRF and CROCO: Northwestern Atlantic of 24~50 $^\circ$ N and 85~45 $^\circ$ W with a spatial resolution of 0.075 $^\circ$. The global time step was 360 s, and the source term time step was 10 s. The spectral discretization of WW3 was 36 divisions for the direction (every 10 $^\circ$) and 35 for the frequency. The surface wind and sea-ice content derived from 6-hourly CFSv2 forced the wave model. The spin-up run was computed for two weeks until 00:00 UTC 01 January 2018. The lateral boundary conditions for the domain were the wave model in the whole Atlantic. The wave model was computed with meridional 0.25 $^\circ$ and zonal 0.2 $^\circ$ resolutions from 01 to 10 January 2018. The spin-up run for the parent domain was computed for the previous December 2017.

3-2. Atmosphere-Wave Interaction

In this study, we configure the coupled model so that the surface roughness and the friction velocity in the atmospheric model are dependent on the surface ocean wave parameters. Here, a part of the boundary layer model of the WRF relevant to this study will be outlined.

The friction velocity u_* is an important parameter that represents the surface stress:

$$u_* = \sqrt{\frac{\tau_a}{\rho_a}} \ , \#(\ \mathrm{SEQ} \quad \backslash * \ \ ARABIC\ 1)$$

where τ_a is the surface stress, and ρ_a is the air density. The surface aerodynamic roughness length z_0 is a vital parameter that exchanges surface information to the atmosphere in a coupled model. The z_0 is parameterized as:

$$z_0 = \frac{0.11\nu}{u_*} + \alpha\frac{u_*^2}{g} \ , \#(\ \mathrm{SEQ} \quad \backslash * \ \ ARABIC\ 2)$$

where ν is the kinematic viscosity, g is the gravitational acceleration, and α is the Charnock coefficient, equal to 0.0185 without wave coupling. This relation is also called a Charnock relationship. The Charnock coefficient α is a function of ocean wave parameters in this model (discussed later). Though u_* and z_0 are not independent, u_* is calculated first in the model integration procedure. The u_* is calculated as:

$$u_* = k_\nu U(z)\left[\log\left(\frac{z}{z_*}\right) - \psi_m\left(\frac{z}{L}\right)\right] \ , \#(\ \mathrm{SEQ} \quad \backslash * \ \ ARABIC\ 3)$$

where $k_\nu (= 0.4)$ is von-Karman constant, $U(z)$ is the wind speed at the height z in the atmospheric model, L is the Monin-Obukhov length, and ψ_m is the stability function of momentum. The z_0 in Eq.(2) is computed at the previous iteration in the model with u_* in Eq.(1). The time step of the atmospheric model is much shorter than the wave model. Therefore, the atmospheric model well incorporates the status of the ocean waves. The u_* is also associated with the heat flux from the surface. The sensible heat flux Q_S and the latent heat flux Q_L are defined as

$$Q_S = -\rho_a C_p u_* \theta_* = -\rho_a C_p C_k U(z)\left[\theta(z) - \theta_s\right] \ , \#(\ \mathrm{SEQ} \quad \backslash * \ \ ARABIC\ 4)$$

$$Q_L = \rho_a L_e u_* q_* = -\rho_a L_e C_q U(z)\left[q(z) - q_s\right] \ , \#(\ \mathrm{SEQ} \quad \backslash * \ \ ARABIC\ 5)$$

where C_p is the specific heat under constant pressure (=1004 J/K kg), L_e is the latent heat of evaporation, θ is the potential temperature, and q is the specific humidity. The subscript s (lower case) indicates a value at the surface. C_k is the sensible heat transfer coefficient, and C_q is the latent heat transfer coefficient, and they are affected by the wave conditions through u_*.

The wave information is passed to the atmosphere via the Charnock coefficient α:

$$\alpha = \frac{0.01}{\sqrt{1 - \frac{\tau_w}{\tau_a}}} \ , \#(\ \mathrm{SEQ} \quad \backslash * \ \ ARABIC\ 6)$$

where τ_w is the wave-induced stress defined as:

$$\tau_w = \rho_w \int_0^{\infty} \int_{-\pi}^{\pi} \sigma^2 S_{\text{in}} \frac{\mathbf{k}}{k} d\theta d\sigma \ , \#(\text{ SEQ } \quad \backslash * \ ARABIC \ 7)$$

where ρ_w is the water density, σ is the wave frequency, θ is the wave direction, and S_{in} is the input source term. The S_{in} is calculated with the method ST4 option of the WW3 in this study (cf. Ardhuin et al. 2010).

In addition to the wave-induced stress, misalignment of the direction of wave and wind is taken into account. Patton et al. (2019) constructed an atmospheric large-eddy simulation model following Sullivan et al. (2014) and investigated the relationships among atmospheric turbulence, wave propagating direction, and wave age. They found that the wave direction and wave age significantly influence the wind vertical profile and turbulence because the swell generates wave-induced turbulence in the atmospheric boundary layer. They suggested modifying the friction velocity u_{*w} with the wave direction and age as

$$u_{*w} = u_* \left(1 + \gamma w_{\text{age}} \left[1 - \cos\phi\right]\right), \#(\text{ SEQ } \quad \backslash * \ ARABIC \ 8)$$

where w_{age} is the wave age defined by $\frac{c_p}{u_*}$, ϕ is the relative angle of the wave to the surface wind, and γ is a constant parameter equal to 0.007. Patton et al. (2019) reported that replacing the original u_* with u_{*w} in the WRF model leads to an improved vertical wind profile above the sea.

Although previous studies have investigated the influences of wave coupling on the atmosphere, how wave coupling affects the explosive cyclone and the turbulent boundary layer is still unclear. Note that the current study does not consider the impacts of sea spray to clarify the influence of the ocean waves themselves on explosive cyclone development.

3-3. Wave-induced Mixing

Our experiment examined how wave-induced mixing affects the ocean field with an explosive cyclone. It is expected that grown waves by the explosive cyclone should enhance the ocean vertical mixing and transform the ocean thermal structure. We applied the non-breaking wave-induced ocean mixing effects into the coupled model. The wave-induced mixing was introduced into the turbulent momentum governing equations in the CROCO model. In this study, the CROCO adopted the GLS (generic length scale) approach, which is a kind of turbulence second-order closure scheme to parameterize turbulent momentum flux. In this research model, the Mellor-Yamada level 2.5 (MY25) scheme is assigned (Mellor & Yamada, 1982). The wave-current interaction that we focus on is the turbulence effects on the internal ocean by surface waves.

In the ocean model, a new term of the non-breaking wave-induced mixing P_{wave} was appended to the existing shear production P in the turbulent momentum

governing equations, as suggested by Babanin (2011). The original shear production term P is defined as

$$P = -\overline{u'w'}\frac{\partial u}{\partial z} - \overline{v'w'}\frac{\partial v}{\partial z} = K_M\left[\left(\frac{\partial u}{\partial z}\right)^2 + \left(\frac{\partial v}{\partial z}\right)^2\right], \#(\text{ SEQ } \backslash * \ ARABIC\ 9)$$

where (u, v, w) is the current velocity, (u', v', w') is the turbulent velocity, and K_M is the eddy viscosity. The overbar represents the Reynolds-averaged value. The modified shear production term $P + P_{\text{wave}}$ is used in the coupled model's GLS scheme. According to Ghantous and Babanin (2014a), the new term P_{wave} is defined as

$$P_{\text{wave}} = bk\left(\frac{\omega H_s}{2}e^{\text{kz}}\right)^3, \#(\text{ SEQ } \backslash * \ ARABIC\ 10)$$

where $b(= 0.0014)$ is an empirical constant following Babanin (2017), k is the wavenumber, ω is the peak angular frequency, H_s is the significant wave height, and z is the water depth. This formulation was derived from laboratory experiments and numerical simulations. The method assumes that the turbulence dissipation by the non-breaking waves should be equal to the turbulence production rate (Huang & Qiao, 2010). The method also assumes that all energy dissipated by non-breaking waves goes into turbulence production. With the new term P_{wave}, the wave-induced mixing effect was appended to the eddy viscosity K_M. In high-grown waves under the explosive cyclone, the ocean mixing is expected to be enhanced, and the boundary layer behaviors transform.

Table 1. Setups of the six sensitivity experiments. CFSv2 is provided as the off-line external forcing.

Experiments	**Atmosphere (WRF)**	**Wave (WW3)**	**Ocean (CROCO)**
A		—	SST (CFSv2)
AW			
O	Wind, EP, Radiation (CFSv2)	—	
WO			
AO		—	
AWO			

Table 2. Coupled variables among the elemental models and their detailed explanations. The first column is the sender of the variables, and the second column is the receiver.

Model (send)	Model (receive)	Exchange variables
WRF	CROCO	(x, y) : Surface stress $[N/m^2]$
		W: EP flux $[kg/m^2 s]$
		R_L: Longwave radiation $[W/m^2]$
		R_S: Shortwave radiation $[W/m^2]$
	WW3	$\mathbf{U_{10}}(x, y)$: Wind speed at 10 m height $[m/s]$
CROCO	WRF	SST: Sea surface temperature [℃]
		$\mathbf{u_{c0}}(x, y)$: Current velocity $[m/s]$
	WW3	η: Water level $[m]$
		$\mathbf{u_{c0}}(x, y)$: Current velocity $[m/s]$
WW3	WRF	α: Charnock coefficient
		f_p: Wave peak frequency $[/s]$
		θ_m: Wave mean direction
	CROCO	T_m: Wave mean period $[s]$
		H_s: Significant wave height $[m]$
		θ_m: Wave mean direction
		$_{\mathbf{w}}(x, y)$: Wave stress $[N/m^2]$

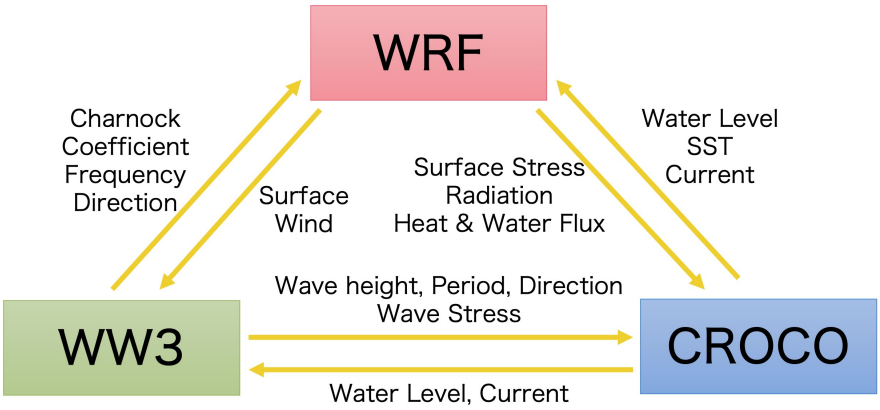

Fig 3. Schematic diagram of the coupled model and exchanged variables.

4 Results of Fully Coupled Simulation

The evolution of the explosive cyclone was successfully reproduced in the fully coupled simulation (AWO). From 0:00 UTC on 04 January, the cyclone's central SLP dropped from 994 hPa to 947 hPa (-47 hPa) in 24 hours and reached 942 hPa at 4:00 UTC on 05 January (bottom figure in Fig 1). Although the decrease in the cyclone central pressure in the AWO experiment was slightly greater than that in the CFSv2 data, the experiment successfully reproduced the timing of the rapid intensification of the explosive cyclone. The reproduced trajectory was well traced to the CFSv2 data (Fig 4), meaning that the wave coupling does not significantly shift the cyclone's trajectory.

The delay of the temporal development in the wave height against the wind speed was discovered by Kita et al. (2018), which is a feature of the wave development under explosive cyclones. Because the explosive cyclone propagated forward at a higher speed than the wave propagation speed, the evolution of the ocean wave height lagged behind the wind speed growth by hours. Fig 5 illustrates the temporal developments of the surface wind speed at 10 m height U_{10} and significant wave height H_s around which the explosive cyclone developed most maturely from 18:00 on 04 January to 6:00 on 05 January. The central SLP deepened most deeply at 4:00 UTC on 05 January. Even though U_{10} around the center remained unchanged during the 12 hours, H_s evolved sharply with the time elapse. The time lag between the evolutions of wind and ocean surface waves is unique to explosive cyclones.

The sensible and latent heat supply from a warm ocean current facilitates the vertical atmospheric convection and enhances the development of the explosive cyclone. As illustrated in Fig 6a, a massive amount of sea surface heat was supplied around the Gulf Stream along the U.S. east coast. Fig 6b demonstrates that the evolving surface wave amplified z_0 around the cyclone center where H_s got sufficiently high. The heat supply from the sea surface was determined by the wind speed, temperature, humidity differences, and the transfer coefficient, according to Eq.(4) and (5). The transfer coefficient depends on z_0.

The ocean mixed layer depth (MLD) decides how much marine heat can be transferred to the atmosphere. The MLD deepened on the southern side of the Gulf Stream (Fig 6c). The wave-induced mixing implemented in this study is expected to alter the vertical ocean mixing (expressed by K_M as in Fig 6d), transform MLD, and influence the internal ocean heat structure. The effect of the wave-induced mixing on the internal ocean will be discussed in Section 5.3.

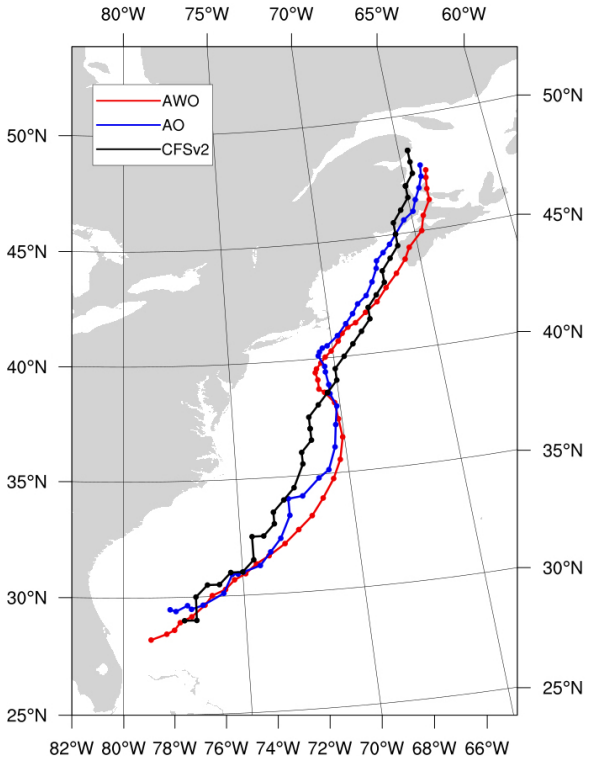

Fig 4. The trajectories of the cyclone center for the AWO (red) and the AO (blue) simulations, and CFSv2 (black) from 18:00 UTC on 03 January to 18:00 UTC on 05 January. The dots are plotted every hour.

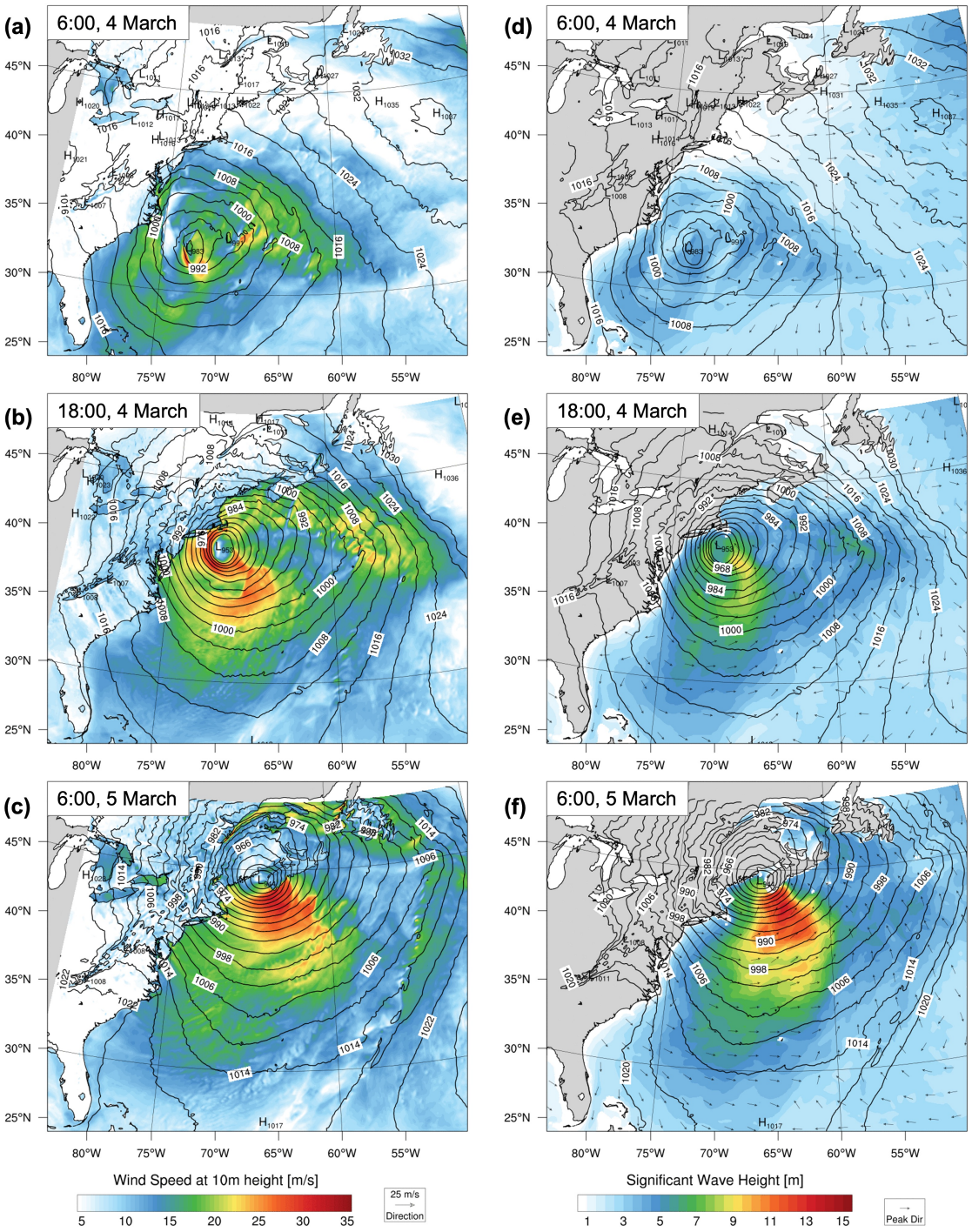
(a)
6:00, 4 March
(b)
18:00, 4 March
(c)
6:00, 5 March
(d)
6:00, 4 March
(e)
18:00, 4 March
(f)
6:00, 5 March
45°N
40°N
35°N
30°N
25°N
80°W
75°W
70°W
65°W
60°W
55°W
Wind Speed at 10m height [m/s]
5
10
15
20
25
30
35
25 m/s
Direction
Significant Wave Height [m]
1
3
5
7
9
11
13
15
Peak Dir

Fig 5. Horizontal distributions of (a) U_{10} (m/s; shaded) and (b) H_s (m; shaded) in the AWO simulation at 6:00 and 18:00 UTC on 04 January, at 6:00 UTC on 05 January. The SLP contour (solid black) interval is 4 hPa.

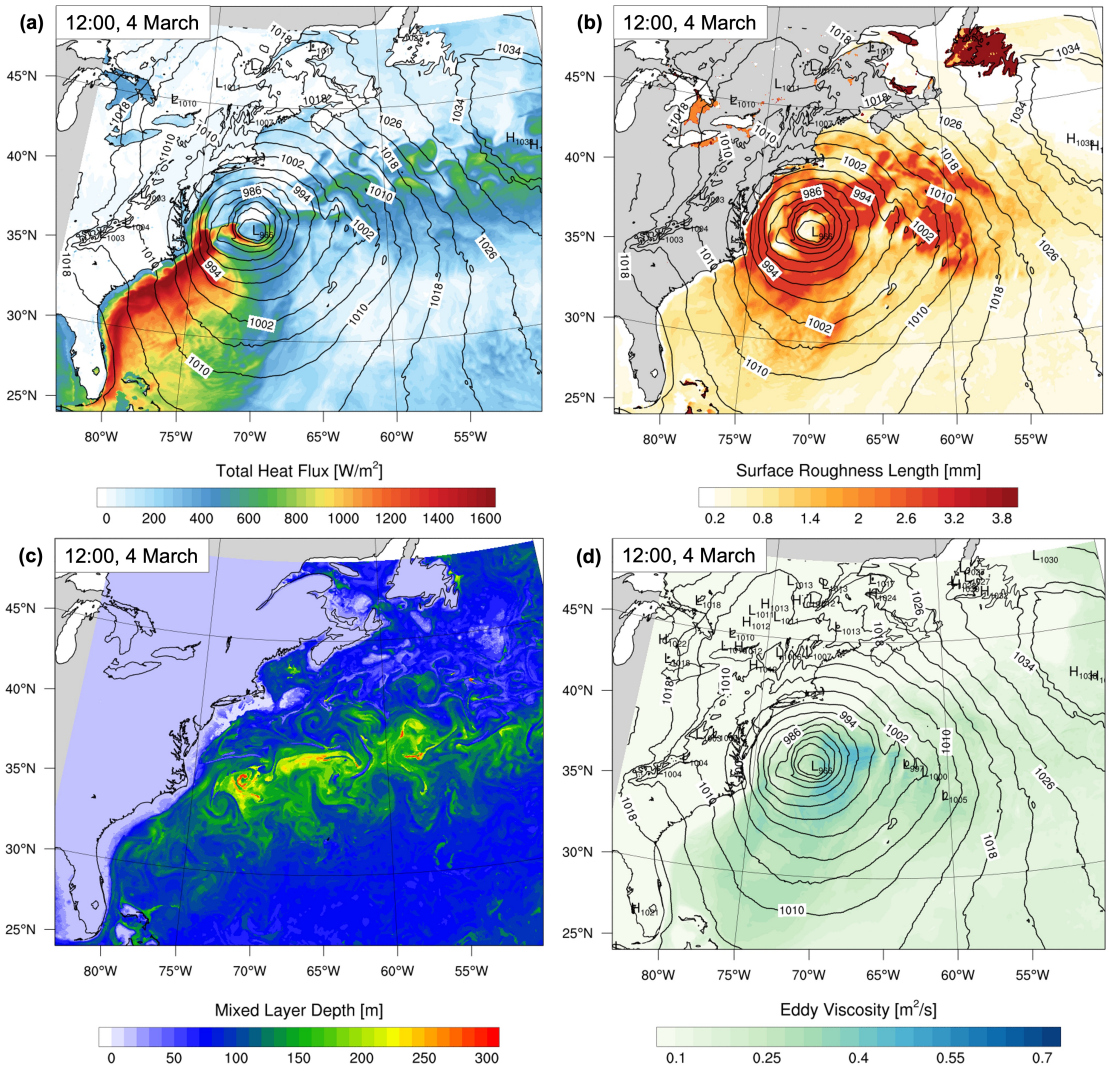

Fig 6. Horizontal distributions of (a) $\mathrm{HF}_{\mathrm{total}}$ (shaded; W/m^2), (b) θ_e (shaded; K), (c) MLD (shaded; m), and (d) K_M (shaded; m^2/s) in the AWO simulation at 12:00 UTC on 04 January. The SLP contour interval is 4 hPa.

4-1. Reproducibility of fully coupled simulation

The reproducibility of the wind speed and SLP in the AWO experiment was significantly improved compared to the AO experiment. The marine buoy data in the Northwestern Atlantic were analyzed to verify the numerical simulations'

accuracy (AWO and AO); eight buoy observations were selected for comparison. The observation data was collected by the National Data Buoy Center (NDBC; https://www.ndbc.noaa.gov/) and the Environment and Climate Change Canada (http://www.meds-sdmm.dfo-mpo.gc.ca/isdm-gdsi/index-eng.html). The locations of these buoys are shown in Fig 7. These buoys were selected because of their proximity to the trajectory of the explosive cyclone, as well as their availability during the cyclone emergence. The simulation comparisons with the observations were carried out at hourly intervals to match the numerical simulation output intervals. The data was subsampled into hourly intervals when the observation intervals were 10 minutes. The H_s time-series of the observation and the AWO experiment results at the LaHave Bank location (42.5 ° N, 64.02 ° W; 1300 m depth) are illustrated in Fig 8. Overall, the simulation well reproduced the observed H_s. The bias and the correlation coefficient during the nine days are -0.8 m and 0.86, respectively. The biases at the other locations are within 0.8 m, and the correlation coefficients are over 0.85. Consequently, the wave simulation showed excellent agreement with the observations.

The surface wind speed and the SLP were analyzed for all eight locations. The Taylor diagrams describe the skills of each model for the observations, as illustrated in Fig 9. The surface wind speed simulation results were fitted to the anemometer height of each location with the Monin-Obukhov similarity theory. The surface wind speed analysis illustrated that the simulations well reproduced the observations, and the AWO performance was superior to the AO. The correlation coefficient at every point during the nine days was over 0.95. The reproducibility for the SLP of both simulations was also considerably high; hence the AWO performance was higher than the AO. This is because the changes of the heat and momentum exchanges on the air-sea interface, induced by the ocean surface waves, affected the free atmosphere. This consequence indicates that ocean surface waves play a significant role in developing the explosive cyclone. The detailed mechanism is discussed in the next section.

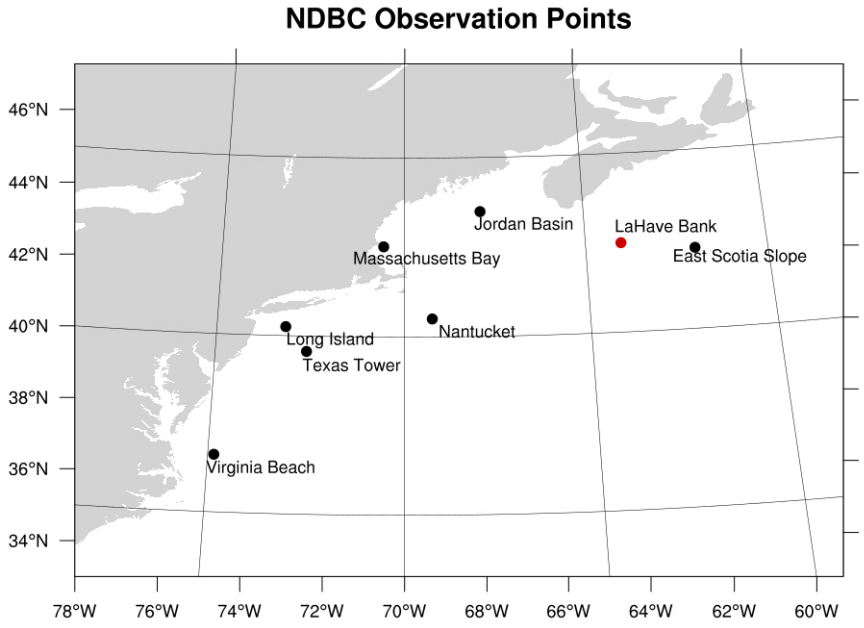

Fig 7. Geographical locations of the eight observation buoys in the Northwestern Atlantic.

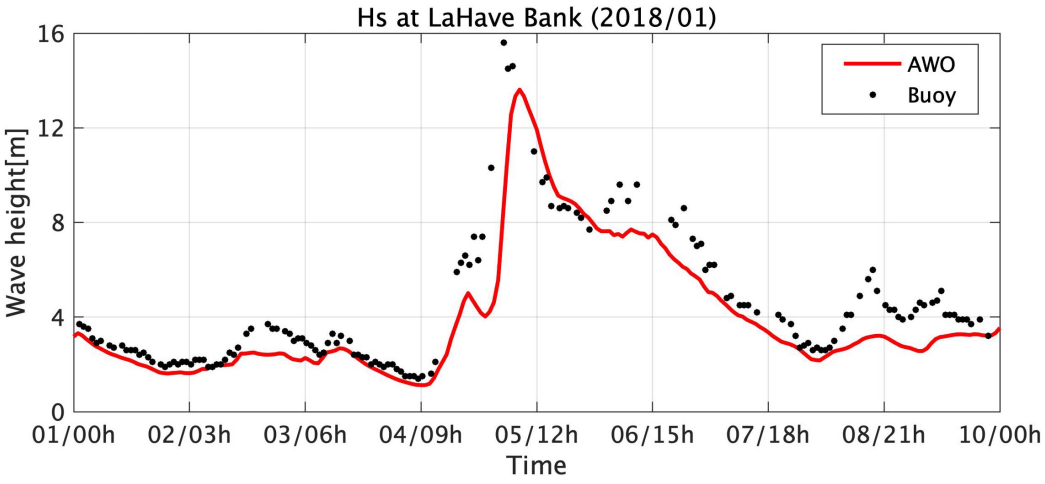

Fig 8. Time-series of H_s [m] at the LaHave Bank buoy location. The red line represents the AWO experiment, while the black dots represent the observation.

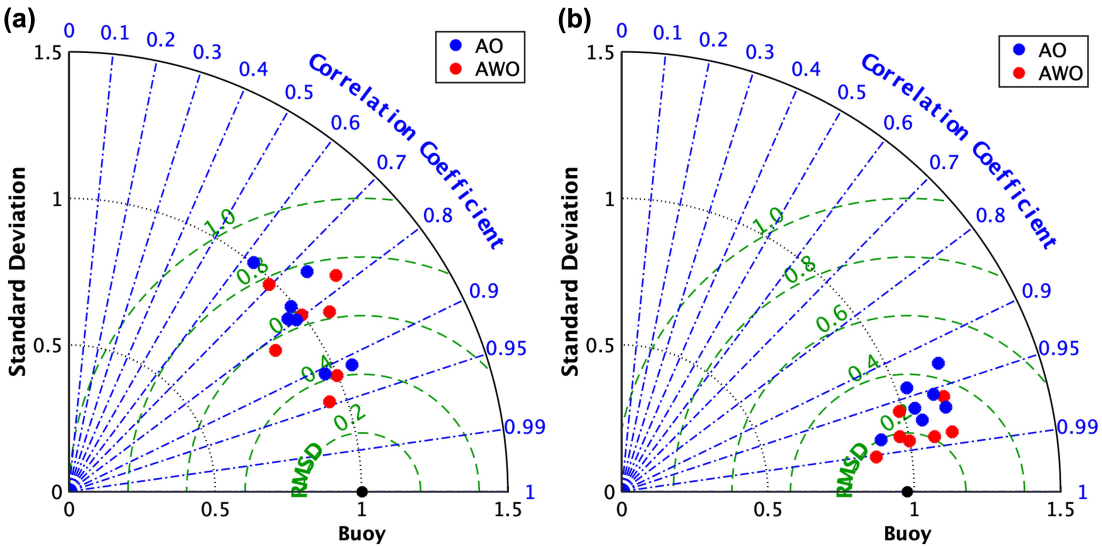

Fig 9. Taylor diagrams for the observed parameters: (a) the surface wind speed [m/s] and (b) SLP [hPa] with the AWO (red dots) and AO (blue dots) experiments. The data is normalized by the standard deviation of the buoy observation data.

5 Discussions

The wave coupling made notable changes in the explosive cyclone development and the underlying ocean. This section explains the detailed changes and clarifies the mechanisms derived by the wave coupling.

5-1. Wave-driven Changes in Explosive Cyclone Development

The wave coupling to the atmosphere-ocean coupled model moderately deepened the central SLP of the explosive cyclone. The lowest central SLP in the AWO experiment was deeper by 2 hPa than the AO experiment at 4:00 UTC on 05 January (Fig 1b). Fig 10a shows that the total amount of sensible and latent heat flux from the sea surface significantly increased around the cyclone center in the AWO compared to the AO during the rapid cyclone development (12:00 UTC on 04 January). HF_{total} is defined as the area-averaging of sensible and latent heat flux in the square area bounding with 82 ˚ W-60 ˚ W and 25 ˚ N-45 ˚ N. This HF_{total} stands for an amount of heat that the explosive cyclone obtained from the ocean. The HF_{total} in the AWO experiment exceeded that in the AO during the cyclone advent (Fig 11a). On the other hand, U_{10} under the cyclone declined in the AWO experiment compared to the AO (Fig 11b). This decline is caused by the increase in the sea surface friction derived from the wave coupling. The mechanisms of how the surface heat flux increased and the wind speed decreased will be discussed in detail in Section 5.2.

The SST changed significantly with the wave coupling, as shown in Fig 10b. The

SST south of the Gulf Stream cooled down, while the SST north of the Gulf Stream warmed up. This division can be attributed to the vertical temperature profile in the internal ocean. The SST warmed up in the north of the Gulf Stream with the temperature inversion (type-I profile), while the SST cooled down in the south of the Gulf Stream with the typical temperature profile (type-T). The wave mixing effect intensified the vertical mixing in the ocean mixed layer (details in Section 5.3).

The SST cooling south of the Gulf Stream decreases the heat supply from ocean to atmosphere, while the SST warming north of the Gulf Stream does the opposite. Since the total heat amount $\mathrm{HF}_{\mathrm{total}}$ from ocean to atmosphere consequently increased in the AWO experiment against the AO, the SST cooling effect on $\mathrm{HF}_{\mathrm{total}}$ was insignificant compared to the other wave-induced effects. The factors affecting the enhanced $\mathrm{HF}_{\mathrm{total}}$ are the wave-intensified roughness and consequent enhancement in the heat transfer coefficient, and will be discussed in Section 5.2

The atmospheric thermal parameter changed significantly with the amplified surface sensible and latent heat supply. To evaluate the effects of the enhanced heat supply from the ocean with the wave-induced interactions in the AWO experiment, the equivalent potential temperature θ_e vertical profile around the cyclone center was investigated. Fig 12 illustrates the time evolution of vertical profiles of θ_e in AWO experiment and θ_e difference between AWO and AO around the cyclone center from the sea surface to 600 hPa level. The averaging area is defined as a $5^\circ \times 5^\circ$ square whose center coincides with the cyclone center. During the rapid development of the explosive cyclone between 0:00 and 18:00 UTC on 04 January (Fig 1a) in the AWO experiment, θ_e in the low troposphere around the cyclone center was warmed by ample sensible and latent heat supply from the sea surface, and the convectively unstable condition was strengthened (Fig 12a). Fig 12b shows that θ_e in the AWO experiment was much higher than that in the AO not only near the surface but also over the middle troposphere (~600 hPa level). An intense updraft occurred in front of the warm front and circulated counterclockwise around the cyclone center. The θ_e warming spread vertically because the intense updraft near the bent-back front lifted high θ_e air on the surface. Consequently, the thermal condition in the middle troposphere around the cyclone center became convectively unstable. The convective instability stimulates the vapor condensation and latent heat release in the explosive cyclone. During the rapid development, the precipitation around the cyclone center (same $5^\circ \times 5^\circ$ square as the θ_e calculation) in the AWO experiment was also amplified compared to the AO (Fig 13). As Hirata et al. (2015) demonstrated, the enhanced unstable condition intensifies the release of latent heat around the bent-back front. The consequent latent heat produces positive potential vorticity and intensifies the rapid development of

the explosive cyclone. The intense condensation of vapor led to intense precipitation and decreased θ_e. After the rapid development of the cyclone, the reduction of θ_e in the AWO was larger than the AO due to more precipitation (Fig 12b).

In summary, the wave-coupling effects in the fully coupled experiment strengthened convectively unstable conditions near the surface with larger heat supply from the sea surface to the atmosphere, strengthened precipitation and latent heating around the center, and finally, intensified the explosive cyclone development. The wave-coupling effects should play an important role in the explosive cyclone development since they helped the numerical simulation reproduce the explosive cyclone more precisely, as mentioned in Section 4.

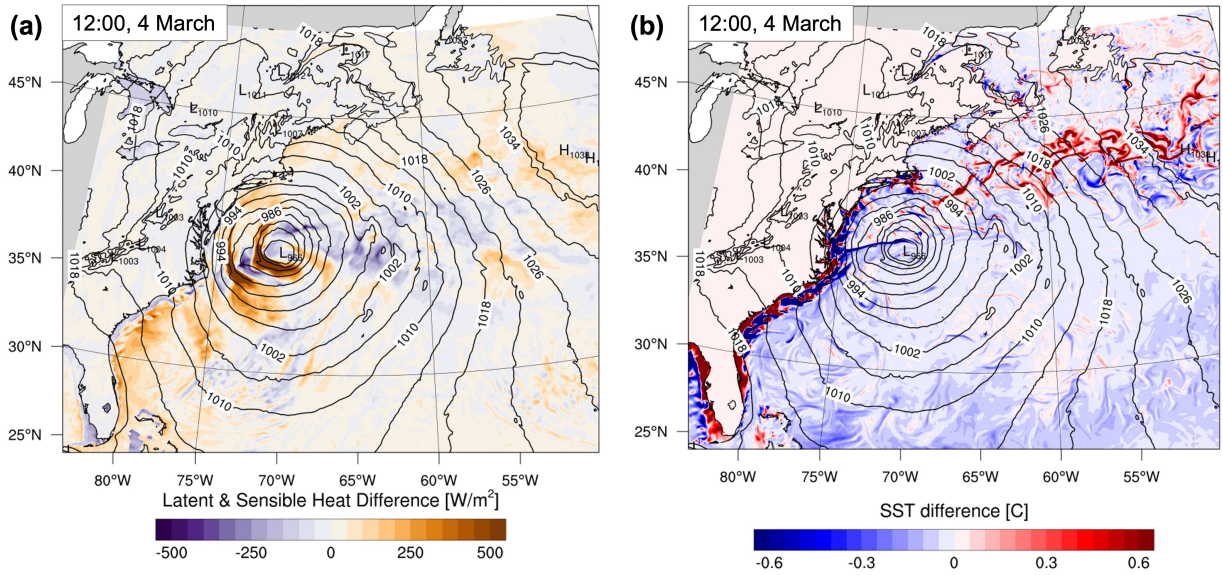

Fig 10. Horizontal distributions of the difference (AWO minus AO) in (a) $\mathrm{HF}_{\mathrm{total}}$ (shaded; W/m^2) and (b) SST (shaded; ℃) at 12:00 UTC on 04 January. The SLP contour interval is 4 hPa.

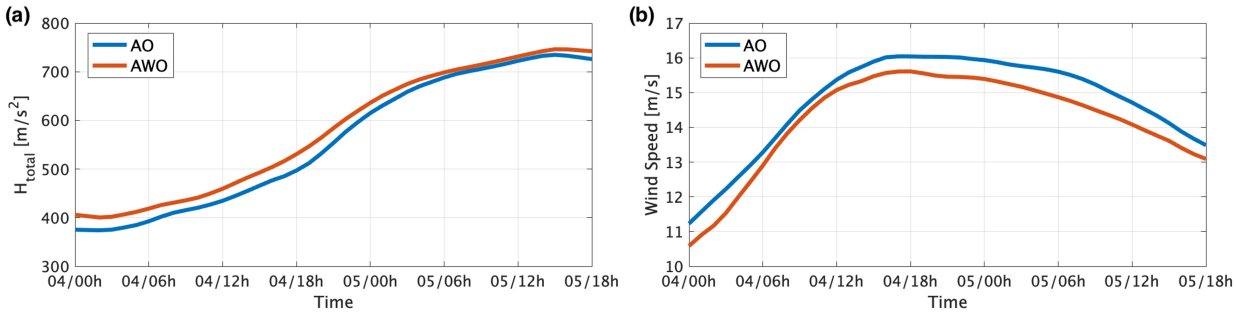

Fig 11. Time-series of (left) the area-averaged $\mathrm{HF}_{\mathrm{total}}$ $[W/m^2]$ and (right) the

area-averaged U_{10} [m/s] in the square area bounding with 82 ° W-60 ° W and 25 ° N-45 ° N for the AWO (red line) and the AO (blue line) experiments.

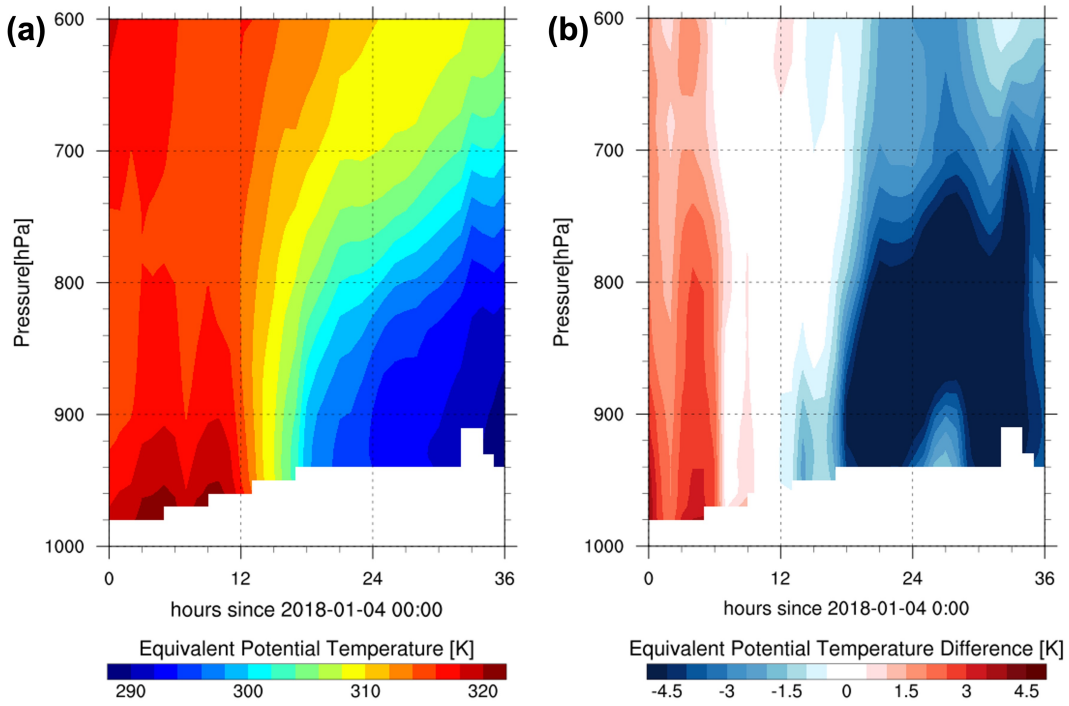

Fig 12. Time evolution of vertical profiles of (a) θ_e [K] in AWO experiment and (b) θ_e difference (AWO minus AO) around the cyclone center from the sea surface to 600 hPa height. It covers the time period from 0:00 UTC on 04 January to 18:00 UTC on 05 January.

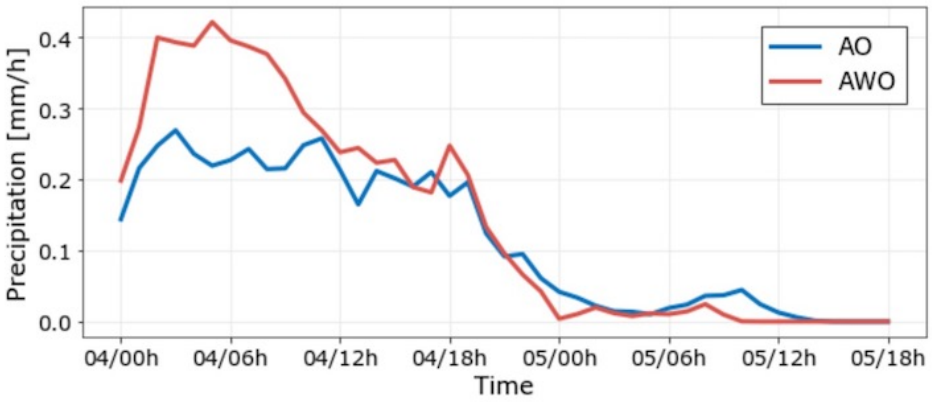

Fig 13. Time-series of precipitation [mm/h] around the cyclone center for the

AWO (red line) and the AO (blue line) simulations.

5-2. Effect of Atmosphere-Wave Coupling

The generation of the ocean surface wave modifies the surface roughness and changes the atmosphere and the internal ocean through air-sea interactions. Comparing the A and AW experiments clarifies how the wave directly changed the atmosphere and resulted in the intensification of the explosive cyclone. Fig 14 displays the relationships z_0 and C_k with U_{10} at 0:00 on 05 January in the same wind bin (3 m/s). In the wave coupling (AW) experiment, z_0 defined by equation (2) was affected by ocean waves via the wave-affected friction velocity u_{*w} (equation (8)) and the Charnock coefficient α (equation (6)). Without the wave coupling, friction velocity was calculated with equation (3), and the Charnock coefficient is $\alpha = 0.0185$. The sensible heat transfer coefficient C_k is derived from equation (4),

$$C_k = \frac{u_* \theta_*}{U(z)[\theta(z) - \theta_s]} . \#(\text{SEQ} \quad \backslash * \ ARABIC \ 11)$$

The latent heat transfer coefficient C_q is usually equal to C_k. The AW experiment generally shows larger z_0 and C_k than those in the A experiment (Fig 14). This intensified z_0 leads to an increase in the surface friction in all wind speed conditions. The enhanced surface friction brought weaker surface wind speed. As shown in Fig 15b, the surface wind speed around the cyclone center decreased dominantly in the AW experiment. The decrease of the surface wind speed is reasonable compared with the previous research for the case of a tropical cyclone (Pianezze et al., 2018). Therefore, the roughened sea surface in the AW experiment weakened the surface wind speed.

Despite the surface wind speed reduction, the surface heat transfer coefficient C_k was larger in intermediate and high wind speeds ($U_{10} > 4$ m/s) for the AW experiment than the A experiment (Fig 14b). Since the wind speed is usually over 10 m/s under the explosive cyclone, C_k in the AW experiment generally overwhelmed C_k in the A experiment. The surface heat flux $\mathrm{HF}_{\mathrm{total}}$ from the ocean to the atmosphere is proportional to U_{10} and C_k. Although the increase in C_k competed with the decrease in U_{10} due to the enhanced z_0, the consequent $\mathrm{HF}_{\mathrm{total}}$ was generally larger in the AW experiment than the A experiment at 12:00 on 04 January (Fig 15a). This tendency was maintained entirely during the explosive cyclone advent, which corresponds to the comparison between the AWO and AO, as shown in Fig 11a. $\mathrm{HF}_{\mathrm{total}}$ increased in the cyclone center's southern area and declined slightly in the eastern area of the cyclone center. The total amount of $\mathrm{HF}_{\mathrm{total}}$ consequently was augmented during the cyclone advent in the AW experiment compared to the A experiment (not shown). U_{10} generally decreased when the wave coupling was active at 12:00 UTC on 04 January (Fig 15b). Although several areas had stronger U_{10} in the AW experiment compared to the A experiment, U_{10} weakened in most areas with the enhanced z_0 in the AW experiment. The area-average wind speed under the explosive cyclone

decreased in the AW experiment, corresponding to the comparison between the AWO and AW experiments (Fig 11a).

The same explanation applies when comparing the AWO and AO experiments, as demonstrated in Section 5.1. The C_k alternation enhanced the sea surface sensible and latent heat transfer into the lower atmosphere in the AWO experiment. The sensible and latent heat flux amplification from the sea surface generated convectively unstable conditions in the surface atmospheric layer. This effect should mainly intensify the explosive cyclone development in the fully coupled model.

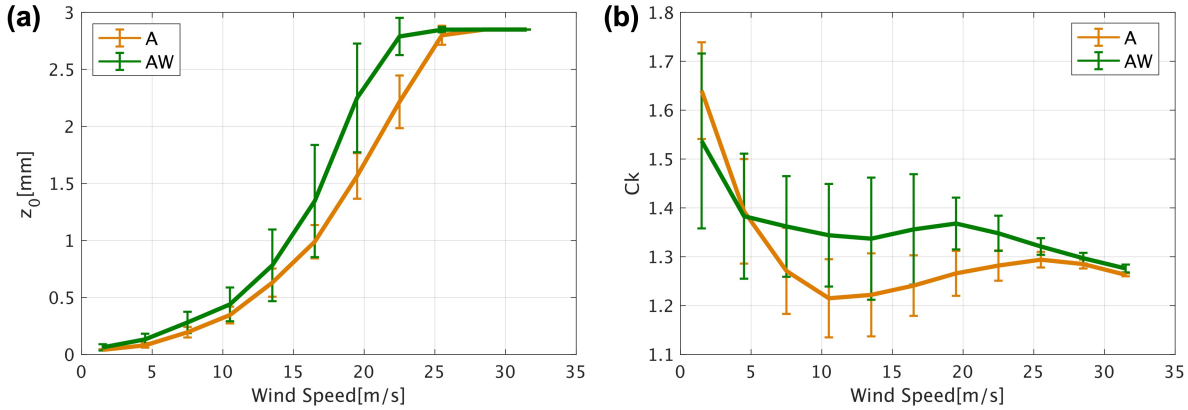

Fig 14. Relationships (a) z_0 [mm] and (b) C_k with U_{10} [m/s] at 0:00 UTC on 05 January. The error bars represent the standard deviations. The lines represent the A (orange) and the AW (green) experiments.

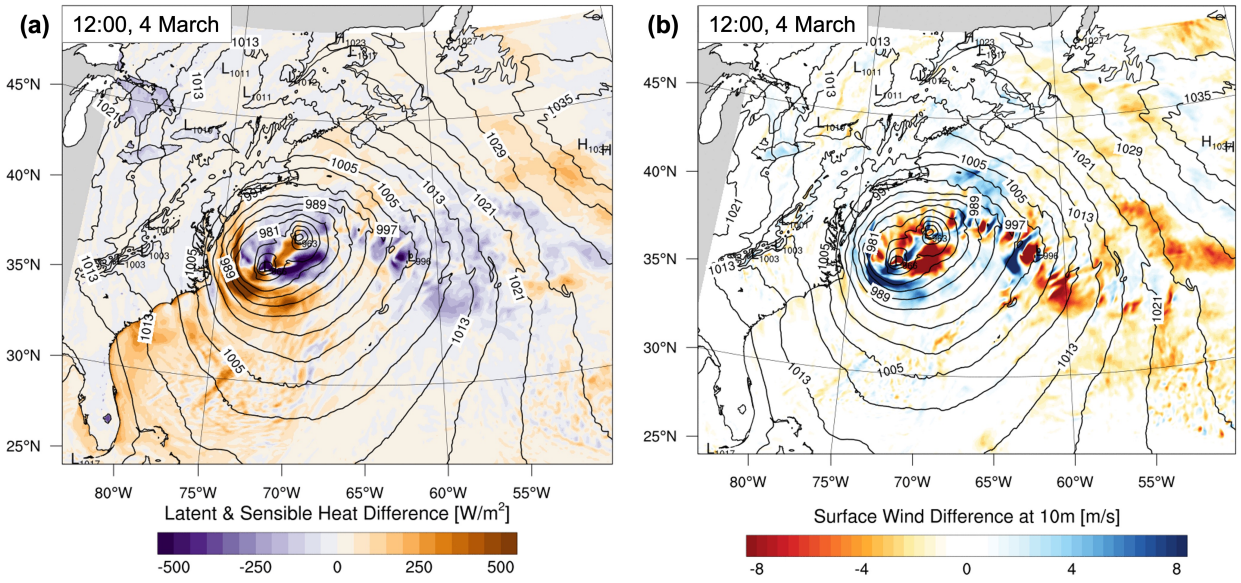

Fig 15. Horizontal distributions of the difference (AW minus A) in HF_{total} (shaded; W/m^2) at 12:00 UTC on 04 January. The SLP contour interval is 4 hPa.

5-3. Effect of Wave-Induced Mixing

The SST changes (Fig 10b) between the AWO and AO experiments indicated that the wave-induced mixing transformed the internal ocean thermal structure under the explosive cyclone. To clarify how the wave-induced mixing changed the SST, the sensitivity experiment without the atmosphere model was implemented: the WO and O experiments.

In Fig 16a, almost the same feature in the SST changes were verified between the WO and O experiments as Fig 10b: the SST south of the Gulf Stream cooled down, while the SST north of the Gulf Stream warmed up. These SST changes were derived from the strengthened wave-induced mixing implemented with the wave-induced shear production P_{wave} (equation (10)). As shown in Fig 16b, the eddy viscosity K_M was remarkably amplified due to the activated wave-induced mixing, which indicates that the ocean vertical mixing was strengthened near the surface. This mixing effect seemed to spread in the broad vertical range because the MLD was also generally deepened in the entire WO domain compared to the O experiment (Fig 16c).

The vertical profile of the water potential temperature θ_w was investigated at Point-P (39 ° N, 68 ° W) where the temperature inversion (type-I) was found in Fig 17a. Fig 17b showed that the rapid intensification in the eddy viscosity K_M reached about 80 m depth when the explosive cyclone center passed by at 18:00 on 04 January. With the enhanced vertical mixing, the MLD deepened after the cyclone traveled past the measurement location (Fig 17c). The WO simulated warmer water temperature in the upper mixed layer and cooler temperature at the bottom of the mixed layer. In terms of the K_M, the WO produced much higher values in the mixed layer at Point-P after the EC passed over the location (Fig 17d). The increased magnitudes in K_M are 0.5 m^2/s at most. The vertical mixing intensified as the wave height grew at Point-P when and after the explosive cyclone passed over the point. Therefore, the experiment revealed wave-induced mixing P_{wave} enhanced vertical mixing and deepened the MLD over a broad area. The enhanced mixing impacted the modeled SST significantly, but with differing effects for the thermal profile types; warming and cooling of upper mixed layer temperatures for the type-I and type-T profiles, respectively. The deepening in MLD due to the wave-induced vertical mixing is consistent with the previous study on a tropical cyclone in the Gulf of Mexico (Aijaz et al., 2017; Pianezze et al., 2018). Jenkins et al. (2012) reported corresponding results that the wave-induced mixing enhances vertical mixing and cools SST down under an extratropical cyclone in the north of the U.K.

To summarize, the wave-induced ocean mixing enhanced the vertical mixing under the explosive cyclone, and the SST changes were affected by the deep-located water temperature due to enhanced vertical mixing in the mixed layer.

With the effect of the non-breaking wave-induced mixing, the SST south of the Gulf Stream was cooled down with the type-T temperature profile; the SST north of the Gulf Stream was warmed up with the type-I temperature profile. Note that this ocean-wave coupling does not change the Gulf Stream axis in the short duration investigated during the cyclone advent in this study. The non-breaking wave-induced mixing enhanced the vertical mixing, transformed the ocean mixed layer's vertical structure, but the resultant SST change was not as dominant on the development of the explosive cyclone compared to the enhancement in the sensible and latent heat supply by the ocean surface wave.

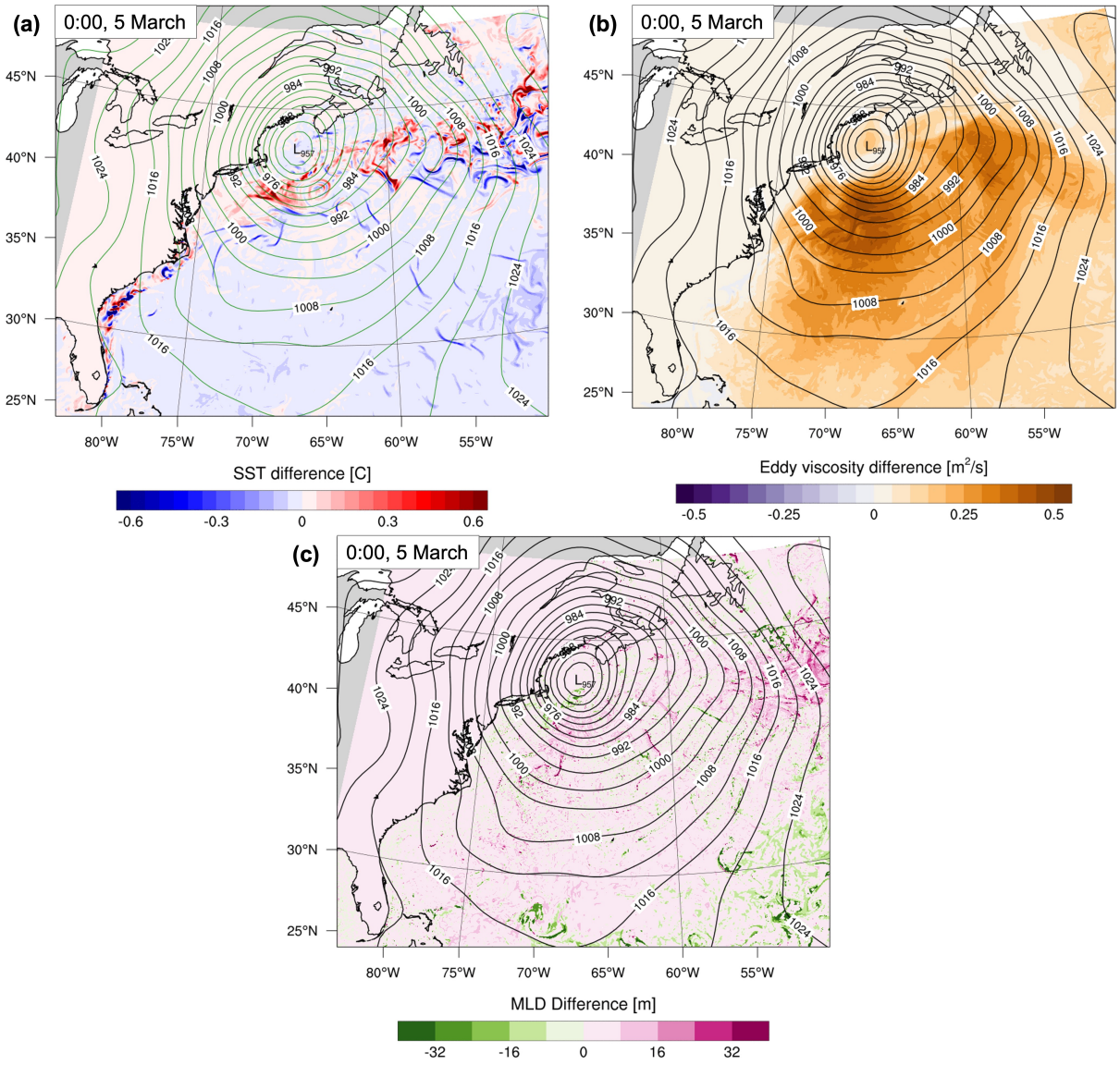

Fig 16. Horizontal distributions of the difference (O minus WO) in (a) SST (shaded; ℃), (b) K_M (shaded; m^2/s) at the first layer of the CROCO, and (c) MLD (shaded; m) at 0:00 UTC on 05 January. The SLP contour interval (solid black) is 4 hPa.

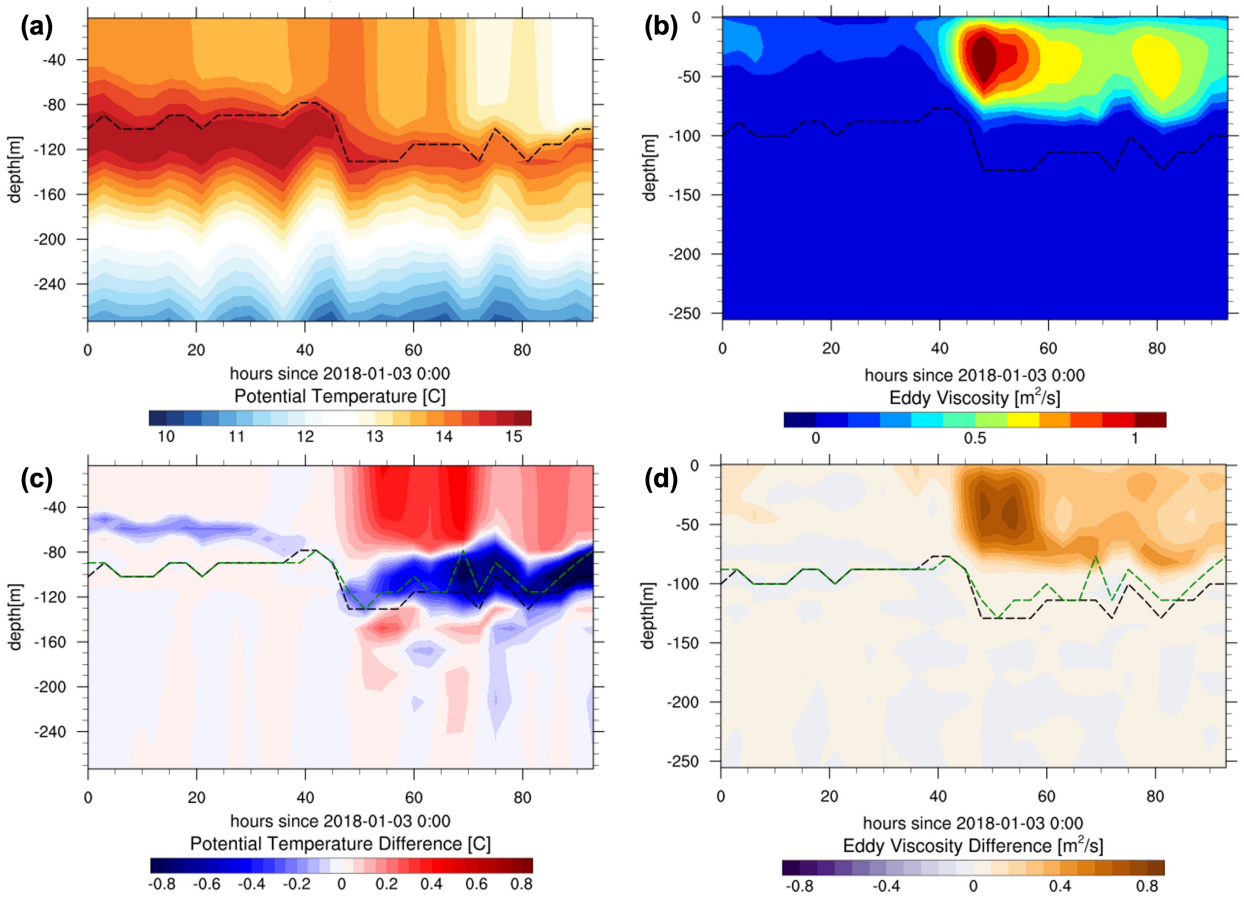

Fig 17. Time evolution of the vertical profile of K_M $[m^2/s]$ difference (WO minus O) at 39 ˚ N, 68 ˚ W. The black dashed line represents the MLD [m] in the WO, and the green one represents that in the O experiment.

6 Summary and Conclusions

This study revealed that the ocean surface waves play a substantial role in intensifying the sensible and latent heat supply from the sea surface and reinforcing the ocean vertical mixing with thermal structure transformation. The integrated effect of these changes intensified the explosive cyclone development. These conclusions were proposed by a coupled atmosphere-ocean-wave model for the explosive cyclone which emerged in the Northwestern Atlantic in January 2018. These wave effects successfully improved the reproducibility of the

explosive cyclone in numerical simulations.

We have shown that the ocean waves enhanced the surface sensible and latent heat supply, and strengthened convective instability and precipitation. In other words, the ocean surface waves significantly affected the mesoscale atmospheric phenomenon through sea surface thermodynamics changes. The ocean surface wave's effect on the explosive cyclone was illustrated in Fig 18. The featured explosive cyclone, generated to the east of Miami, propagated northward along the US east coast with the central SLP deepening. The central SLP reached the lowest value near Massachusetts Bay. The sensible and latent heat supply from the sea surface to the atmosphere increased in the entire region where the cyclone passed. Nevertheless, the oceanic responses were distinct depending on the region due to the internal thermal structure; while the SST south of the Gulf Stream cooled down, the SST north of the Gulf Stream warmed up. Through various sensitivity experiments, the following underlying physical processes were clarified.

The physical processes of the wave impact on the explosive cyclone development are summarized in the schematic diagrams in Fig 19. The coupling process of atmosphere and wave enhanced the sensible and latent heat supply from the sea surface over the entire Northwestern Atlantic and intensified the cyclone development. As the equivalent potential temperature θ_e increased, convective instability was strengthened in the surface-atmosphere layer. The convective instability prevailed up to the middle troposphere and amplified precipitation accompanying latent heating near the bent-back front. Consequently, the increase in latent heating produced positive potential vorticity and deepened the SLP of the explosive cyclone center. Additionally, the surface wind speed declined since the sea surface friction increased due to the enhanced drag coefficient C_d. It is reasonable that the enhanced sensible and latent heat supply associated with the atmosphere-wave-ocean interaction was the most significant factor in intensifying the explosive cyclone's development, corresponding with the previous studies. On the other hand, the ocean and wave coupled processes differed between the north and south regions of the Gulf Stream. The non-breaking wave-induced mixing cooled down the SST south of the Gulf Stream, while the SST warmed up in regions when the cyclone passed over the Gulf Stream because of the temperature inversion layer (type-I). This result agrees with previous studies reporting that the SST response to the developing explosive cyclone is sensitive to vertical mixing. Despite the reduction of SST in the south of the Gulf Stream, the resultant surface sensible and latent heat supply into the atmosphere was enhanced because the wave impact enhancing the transfer coefficients of heat flux overwhelmed the impact of the SST reduction. We succeeded in improving the reproducibility of the explosive cyclone in numerical simulations by the explicit calculation of wave-induced effects.

The work conducted here is the first step to resolving the surface wave effects on explosive cyclones, and there are still unresolved phenomena in this research area. For example, when the ocean wave's phase speed is faster than the surface

wind speed, the swell generates the upward momentum flux and distorts the wind vertical profile (e.g., Sullivan et al., 2008; Hanley and Belcher 2008). The boundary layer parameterizations used in the atmospheric model usually assume the logarithmic wind profile, but the swell-induced turbulent momentum should invalidate the assumption. Moreover, the sea spray is also another key in this research area. Including the sea spray could bring some improvement in the atmospheric simulation. These aspects should be studied in future works.

This study showed that ocean waves can significantly affect the mesoscale atmospheric circulation through momentum and heat supplies from the sea surface. The waves also exhibited great potential in transforming the thermal structures in the marine boundary layer through enhanced vertical mixing. This study concludes that the wave-induced interactions should be considered to improve numerical weather and ocean predictions in mid-latitude regions.

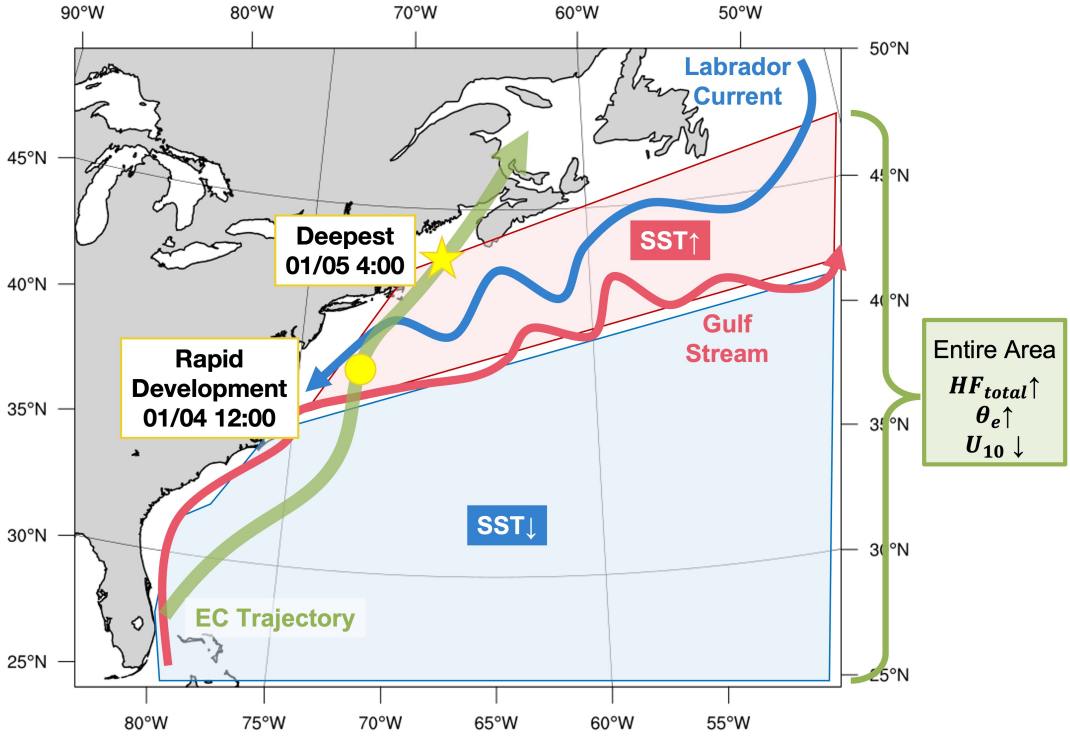

Fig 18. Schematic illustration of the ocean surface wave impacts accompanied by the explosive cyclone in this region.

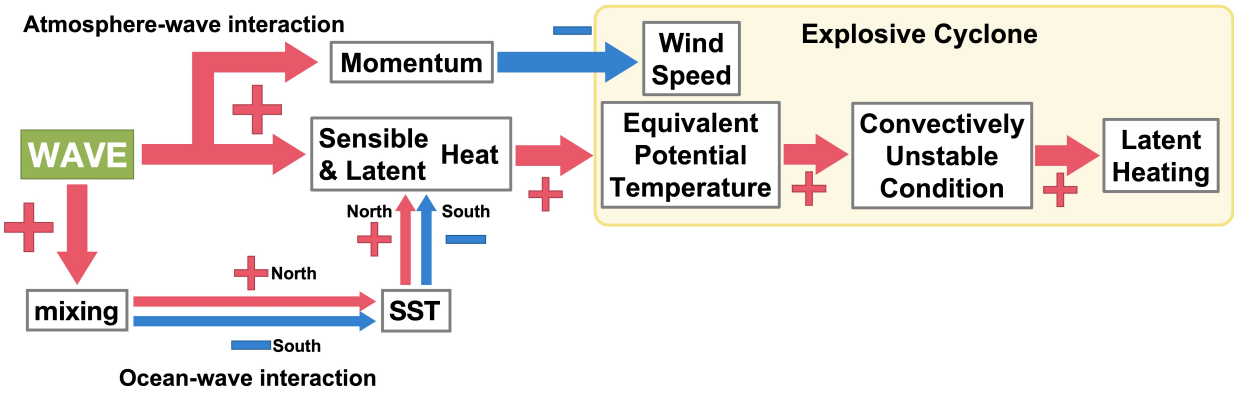

Fig 19. Schematic diagram explains how the ocean waves affect the explosive cyclone development through wave-derived interactions with the atmosphere and the ocean.

Acknowledgments

We would like to thank Roxanne Lai for English language editing. This work was supported by JSPS KAKENHI Grant 17J07627 and 16H01846.

Open Research

Model settings, plotting code, and data used in the study are available online (https://doi.org/10.5281/zenodo.5947601).

References

Aijaz, S., Ghantous, M., Babanin, A. V., Ginis, I., Thomas, B., & Wake, G. (2017). Nonbreaking wave-induced mixing in upper ocean during tropical cyclones using coupled hurricane-ocean-wave modeling. *Journal of Geophysical Research: Oceans*, *122*(5), 3939–3963. https://doi.org/10.1002/2016JC012219Andreas, E. L., Mahrt, L., & Vickers, D. (2012). A New Drag Relation for Aerodynamically Rough Flow over the Ocean. *Journal of the Atmospheric Sciences*, *69*(8), 2520–2537. https://doi.org/10.1175/jas-d-11-0312.1Ardhuin, F., O'Reilly, W. C., Herbers, T. H. C., & Jessen, P. F. (2003). Swell transformation across the continental shelf. Part I: Attenuation and directional broadening. *Journal of Physical Oceanography*, *33*(9), 1921–1939. https://doi.org/10.1175/1520-0485(2003)033<1921:STATCS>2.0.CO;2Ardhuin, F., Rogers, E., Babanin, A. V., Filipot, J.-F., Magne, R., Roland, A., et al. (2010). Semiempirical Dissipation Source Functions for Ocean Waves. Part I: Definition, Calibration, and Validation. *Journal of Physical Oceanography*, *40*(9), 1917–1941. https://doi.org/10.1175/2010JPO4324.1Babanin, A. V. (2011). *Breaking and dissipation of ocean surface waves*. Cambridge University Press.Babanin, A. V., & Makin, V. K. (2008). Effects of wind trend and gustiness on the sea drag:

Lake George study. *Journal of Geophysical Research: Oceans*, *113*(2), 1–18. https://doi.org/10.1029/2007JC004233Battjes, J. A., & Janssen, J. P. F. M. (1978). Energy Loss and Set-Up Due to Breaking of Random Waves. In *Coastal Engineering 1978* (pp. 569–587). New York, NY: American Society of Civil Engineers. https://doi.org/10.1061/9780872621909.034Catto, J. L. (2016). Extratropical cyclone classification and its use in climate studies. *Reviews of Geophysics*, *54*(2), 486–520. https://doi.org/10.1002/2016RG000519Dal Piva, E., Alonso GAN, M., & Cavalcante de Lima MOSCATI, M. (2011). The Role of Latent and Sensible Heat Fluxes in an Explosive Cyclogenesis over the South American East Coast. *Journal of the Meteorological Society of Japan*, *89*(6), 637–663. https://doi.org/10.2151/jmsj.2011-604Dee, D. P., Uppala, S. M., Simmons, A. J., Berrisford, P., Poli, P., Kobayashi, S., et al. (2011). The ERA-Interim reanalysis: Configuration and performance of the data assimilation system. *Quarterly Journal of the Royal Meteorological Society*, *137*(656), 553–597. https://doi.org/10.1002/qj.828Donelan, M. A., Haus, B. K., Reul, N., Plant, W. J., Stiassnie, M., Graber, H. C., et al. (2004). On the limiting aerodynamic roughness of the ocean in very strong winds. *Geophysical Research Letters*, *31*(18), 1–5. https://doi.org/10.1029/2004GL019460Donelan, Mark A., Dobson, F. W., Smith, S. D., & Anderson, R. J. (1993). On the Dependence of Sea Surface Roughness on Wave Development. *Journal of Physical Oceanography*, *23*(9), 2143–2149. https://doi.org/10.1175/1520-0485(1993)023<2143:OTDOSS>2.0.CO;2Dudhia, J. (1989). Numerical study of convection observed during the Winter Monsoon Experiment using a mesoscale two-dimensional model. *Journal of the Atmospheric Sciences*. https://doi.org/10.1175/1520-0469(1989)046<3077:NSOCOD>2.0.CO;2Fairall, C. W., Bradley, E. F., Hare, J. E., Grachev, a. a., & Edson, J. B. (2003). Bulk parameterization of air-sea fluxes: Updates and verification for the COARE algorithm. *Journal of Climate*, *16*(4), 571–591. https://doi.org/10.1175/1520-0442(2003)016<0571:BPOASF>2.0.CO;2Ghantous, M., & Babanin, A. V. (2014). One-dimensional modelling of upper ocean mixing by turbulence due to wave orbital motion. *Nonlinear Processes in Geophysics*, *21*(1), 325–338. https://doi.org/10.5194/npg-21-325-2014Gyakum, J. R., & Danielson, R. E. (2000). Analysis of meteorological precursors to ordinary and explosive cyclogenesis in the Western North Pacific. *Monthly Weather Review*, *128*(3), 851–863. https://doi.org/10.1175/1520-0493(2000)128<0851:AOMPTO>2.0.CO;2Hanley, K. E., & Belcher, S. E. (2008). Wave-driven wind jets in the marine atmospheric boundary layer. *Journal of the Atmospheric Sciences*, *65*(8), 2646–2660. https://doi.org/10.1175/2007JAS2562.1Hasselmann, S., Hasselmann, K., Allender, J. H., & Barnett, T. P. (1985). Computations and Parameterizations of the Nonlinear Energy Transfer in a Gravity-Wave Specturm. Part II: Parameterizations of the Nonlinear Energy Transfer for Application in Wave Models. *Journal of Physical Oceanography*, *15*(11), 1378–1391. https://doi.org/10.1175/1520-0485(1985)015<1378:CAPOTN>2.0.CO;2He, H., & Chen, D. (2011). Effects of surface wave breaking on the oceanic boundary layer. *Geophysical Research Letters*, *38*(7), 1–5. https://doi.org/10.1029/2011GL046665Hirata, H.,

Kawamura, R., Kato, M., & Shinoda, T. (2015). Influential Role of Moisture Supply from the Kuroshio/Kuroshio Extension in the Rapid Development of an Extratropical Cyclone. *Monthly Weather Review*, *143*(10), 4126–4144. https://doi.org/10.1175/MWR-D-15-0016.1Hirata, H., Kawamura, R., Nonaka, M., & Tsuboki, K. (2019). Significant Impact of Heat Supply From the Gulf Stream on a "Superbomb" Cyclone in January 2018. *Geophysical Research Letters*, 2019GL082995. https://doi.org/10.1029/2019GL082995Hong, S.-Y., & Lim, J.-O. J. (2006). The WRF single–moment 6–class microphysics scheme (WSM6). *Journal of the Korean Meteorological Society*, *42*(2).Huang, C. J., & Qiao, F. (2010). Wave-turbulence interaction and its induced mixing in the upper ocean. *Journal of Geophysical Research: Oceans*, *115*(4), 1–12. https://doi.org/10.1029/2009JC005853Janjic, Z. I. (1994). The step-mountain eta coordinate model: further developments of the convection, viscous sublayer, and turbulence closure schemes. *Monthly Weather Review*. https://doi.org/10.1175/1520-0493(1994)122<0927:TSMECM>2.0.CO;2Jenkins, A. D., Paskyabi, M. B., Fer, I., Gupta, A., & Adakudlu, M. (2012). Modelling the effect of ocean waves on the atmospheric and ocean boundary layers. *Energy Procedia*, *24*(January), 166–175. https://doi.org/10.1016/j.egypro.2012.06.098Jiménez, P. A., Dudhia, J., González-Rouco, J. F., Navarro, J., Montávez, J. P., & García-Bustamante, E. (2012). A Revised Scheme for the WRF Surface Layer Formulation. *Monthly Weather Review*, *140*(3), 898–918. https://doi.org/10.1175/MWR-D-11-00056.1Kita, Y., Waseda, T., & Webb, A. (2018). Development of waves under explosive cyclones in the Northwestern Pacific. *Ocean Dynamics*, *68*(10), 1403–1418. https://doi.org/10.1007/s10236-018-1195-zKuo, Y.-H., Low-Nam, S., & Reed, R. J. (1991). Effects of Surface Energy Fluxes during the Early Development and Rapid Intensification Stages of Seven Explosive Cyclones in the Western Atlantic. *Monthly Weather Review*, *119*(2), 457–476. https://doi.org/10.1175/1520-0493(1991)119<0457:EOSEFD>2.0.CO;2Mahrt, L., Miller, S., Hristov, T., & Edson, J. (2018). On Estimating The Surface wind stress over the sea. *Journal of Physical Oceanography*, *48*(7), 1533–1541. https://doi.org/10.1175/JPO-D-17-0267.1Mellor, G. L., & Yamada, T. (1982). Development of a turbulence closure model for geophysical fluid problems. *Reviews of Geophysics*, *20*(4), 851. https://doi.org/10.1029/RG020i004p00851Mlawer, E. J., Taubman, S. J., Brown, P. D., Iacono, M. J., & Clough, S. A. (1997). Radiative transfer for inhomogeneous atmospheres: RRTM, a validated correlated-k model for the longwave. *Journal of Geophysical Research D: Atmospheres*, *102*(14), 16663–16682. https://doi.org/10.1029/97jd00237Nakanishi, M., & Niino, H. (2009). Development of an Improved Turbulence Closure Model for the Atmospheric Boundary Layer. *Journal of the Meteorological Society of Japan*, *87*(5), 895–912. https://doi.org/10.2151/jmsj.87.895Nuss, W. A., & Kamikawa, S. I. (1990). Dynamics and Boundary Layer Processes in Two Asian Cyclones. *Monthly Weather Review*, *118*(3), 755–771. https://doi.org/10.1175/1520-0493(1990)118<0755:DABLPI>2.0.CO;2Oost, W. A., Komen, G. J., Jacobs, C. M. J., & Van Oort, C. (2002). New evidence for a relation between wind stress

and wave age from measurements during ASGAMAGE. *Boundary-Layer Meteorology*, *103*(3), 409–438. https://doi.org/10.1023/A:1014913624535Patton, E. G., Sullivan, P. P., Kosović, B., Dudhia, J., Mahrt, L., Žagar, M., & Marić, T. (2019). On the influence of swell propagation angle on surface drag. *Journal of Applied Meteorology and Climatology*, JAMC-D-18-0211.1. https://doi.org/10.1175/JAMC-D-18-0211.1Perrie, W., Zhang, W., L Andreas, E., Li, W., Gyakum, J., & McTaggart-Cowan, R. (2005). Sea Spray Impacts on Intensifying Midlatitude Cyclones. *Journal of the Atmospheric Sciences*, *62*(6), 1867–1883. https://doi.org/10.1175/JAS3436.1Pianezze, J., Barthe, C., Bielli, S., Tulet, P., Jullien, S., Cambon, G., et al. (2018). A New Coupled Ocean-Waves-Atmosphere Model Designed for Tropical Storm Studies: Example of Tropical Cyclone Bejisa (2013-2014) in the South-West Indian Ocean. *Journal of Advances in Modeling Earth Systems*, 801–825. https://doi.org/10.1002/2017MS001177Powell, M. D., Vickery, P. J., & Reinhold, T. a. (2003). Reduced drag coefficient for high wind speeds in tropical cyclones. *Nature*, *422*(March), 279–283. https://doi.org/10.1038/nature01481Reed, R. J., Grell, G. A., & Kuo, Y.-H. (1993). The ERICA IOP 5 Storm. Part II: Sensitivity Tests and Further Diagnosis Based on Model Output. *Monthly Weather Review*, *121*(6), 1595–1612. https://doi.org/10.1175/1520-0493(1993)121<1595:TEISPI>2.0.CO;2Reichl, B. G., Ginis, I., Hara, T., Thomas, B., Kukulka, T., & Wang, D. (2016). Impact of sea-state-dependent Langmuir turbulence on the ocean response to a tropical cyclone. *Monthly Weather Review*, *144*(12), 4569–4590. https://doi.org/10.1175/MWR-D-16-0074.1Renault, L., Chiggiato, J., Warner, J. C., Gomez, M., Vizoso, G., & Tintoré, J. (2012). Coupled atmosphere-ocean-wave simulations of a storm event over the Gulf of Lion and Balearic Sea. *Journal of Geophysical Research: Oceans*, *117*(9), 1–25. https://doi.org/10.1029/2012JC007924Saha, S., Moorthi, S., Wu, X., Wang, J., Nadiga, S., Tripp, P., et al. (2014). The NCEP climate forecast system version 2. *Journal of Climate*, *27*(6), 2185–2208. https://doi.org/10.1175/JCLI-D-12-00823.1Sanders, F., & Gyakum, J. R. (1980). Synoptic-dynamic climatology of the "bomb." *Monthly Weather Review*, *108*, 1589–1606. https://doi.org/10.1175/1520-0493(1980)108<1589:SDCOT>2.0.CO;2Shapiro, M. A., & Keyser, D. (1990). Fronts, JetStreamsandthe Tropopause. In *Extratropical Cyclones: The Erik Palmen memorial volume* (pp. 167–191). American Meteorological Society.Staneva, J., Alari, V., Breivik, Ø., Bidlot, J. R., & Mogensen, K. (2017). Effects of wave-induced forcing on a circulation model of the North Sea. *Ocean Dynamics*, *67*(1), 81–101. https://doi.org/10.1007/s10236-016-1009-0Stoney, L., Walsh, K., Babanin, A. V., Ghantous, M., Govekar, P., & Young, I. (2017). Simulated ocean response to tropical cyclones: The effect of a novel parameterization of mixing from unbroken surface waves. *Journal of Advances in Modeling Earth Systems*, *9*(2), 759–780. https://doi.org/10.1002/2016MS000878Sullivan, P. P., Edson, J. B., Hristov, T., & McWilliams, J. C. (2008). Large-Eddy Simulations and Observations of Atmospheric Marine Boundary Layers above Nonequilibrium Surface Waves. *Journal of the Atmospheric Sciences*, *65*(4), 1225–1245.

https://doi.org/10.1175/2007JAS2427.1Sullivan, P. P., McWilliams, J. C., & Patton, E. G. (2014). Large-Eddy Simulation of Marine Atmospheric Boundary Layers above a Spectrum of Moving Waves. *Journal of the Atmospheric Sciences*, *71*(11), 4001–4027. https://doi.org/10.1175/JAS-D-14-0095.1Takayabu, I., Niino, H., Yamanaka, M. D., & Fukao, S. (1996). An observational study of cyclogenesis in the lee of the Japan central mountains. *Meteorology and Atmospheric Physics*, *61*(1–2), 39–53. https://doi.org/10.1007/BF01029710Toffoli, A., McConochie, J., Ghantous, M., Loffredo, L., & Babanin, A. V. (2012). The effect of wave-induced turbulence on the ocean mixed layer during tropical cyclones: Field observations on the Australian North-West Shelf. *Journal of Geophysical Research: Oceans*, *117*(C11), n/a-n/a. https://doi.org/10.1029/2011JC007780Tolman, H. L. (2002). Alleviating the Garden Sprinkler Effect in wind wave models. *Ocean Modelling*, *4*(3–4), 269–289. https://doi.org/10.1016/S1463-5003(02)00004-5Valcke, S., Craig, T., & Coquart, L. (2015). *OASIS3-MCT User Guide*.Wada, A., Kohno, N., & Kawai, Y. (2010). Impact of Wave-Ocean Interaction on Typhoon Hai-Tang in 2005. *Sola*, *6A*(SpecialEdition), 13–16. https://doi.org/10.2151/sola.6A-004Wang, P., & Sheng, J. (2016). A comparative study of wave-current interactions over the eastern Canadian shelf under severe weather conditions using a coupled wave-circulation model. *Journal of Geophysical Research: Oceans*, *121*(7), 5252–5281. https://doi.org/10.1002/2016JC011758Warner, J. C., Sherwood, C. R., Arango, H. G., & Signell, R. P. (2005). Performance of four turbulence closure models implemented using a generic length scale method. *Ocean Modelling*, *8*(1–2), 81–113. https://doi.org/10.1016/j.ocemod.2003.12.003William C. Skamarock , Joseph B. Klemp , Jimy Dudhia , David O. Gill , Dale M. Barker , Wei Wang, J. G. P. (2008). *A description of the Advanced Research WRF version 3. NCAR Technical note*.Wu, L., Breivik, Ø., & Rutgersson, A. (2019). Ocean-wave-atmosphere interaction processes in a fully coupled modelling system. *Journal of Advances in Modeling Earth Systems*. https://doi.org/10.1029/2019ms001761Zhang, H., Wu, R., Chen, D., Liu, X., He, H., Tang, Y., et al. (2018). Net Modulation of Upper Ocean Thermal Structure by Typhoon Kalmaegi (2014). *Journal of Geophysical Research: Oceans*, *123*(10), 7154–7171. https://doi.org/10.1029/2018JC014119Zhang, W., Perrie, W., & Li, W. (2006). Impacts of Waves and Sea Spray on Midlatitude Storm Structure and Intensity. *Monthly Weather Review*, *134*(9), 2418–2442. https://doi.org/10.1175/MWR3191.1